

เซลล์แสงอาทิตย์ชนิดสีย้อมไวแสงที่มีชั้นอิเล็กทรอนิกส์ Fe₂O₃/TiO₂, WO₃/TiO₂
หรือชนิด CeO₂/TiO₂



นางสาว ญาสุนันท์ วัฒนสุรวิทย์

ศูนย์วิทยพัชร์พยากร
วิทยานิพนธ์นี้เป็นส่วนหนึ่งของการศึกษาตามหลักสูตรปริญญาวิศวกรรมศาสตรมหาบัณฑิต

สาขาวิชาวิศวกรรมเคมี ภาควิชาวิศวกรรมเคมี

จุฬาลงกรณ์มหาวิทยาลัย
คณะวิศวกรรมศาสตร์ จุฬาลงกรณ์มหาวิทยาลัย

ปีการศึกษา 2551

ลิขสิทธิ์ของจุฬาลงกรณ์มหาวิทยาลัย

DYE SENSITIZED SOLAR CELL WITH $\text{Fe}_2\text{O}_3/\text{TiO}_2$, WO_3/TiO_2 OR $\text{CeO}_2/\text{TiO}_2$
ELECTRODE LAYER



Miss Yasunun Wattanasurawit

A Thesis Submitted in Partial Fulfillment of the Requirements
for the Degree of Master of Engineering Program in Chemical Engineering
Department of Chemical Engineering

Faculty of Engineering

Chulalongkorn University

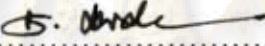
Academic Year 2008

Copyright of Chulalongkorn University

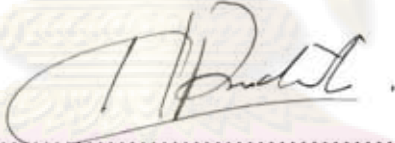
511360

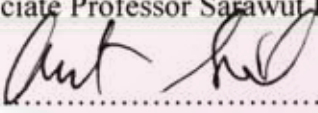
Thesis Title DYE SENSITIZED SOLAR CELL WITH $\text{Fe}_2\text{O}_3/\text{TiO}_2$,
 WO_3/TiO_2 OR $\text{CeO}_2/\text{TiO}_2$ ELECTRODE LAYER
By Miss Yasunun Wattanasurawit
Field of Study Chemical Engineering
Advisor Akawat Sirisuk, Ph.D

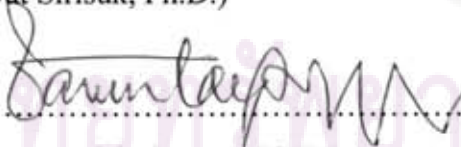
Accepted by the Faculty of Engineering, Chulalongkorn University in
Partial Fulfillment of the Requirements for the Master's Degree


..... Dean of the Faculty of Engineering
(Associate Professor Boonsom Lerthirunwong, Dr. Ing)

THESIS COMMITTEE


..... Chairman
(Associate Professor Sarawut Rimdusit, Ph.D.)


..... Advisor
(Akawat Sirisuk, Ph.D.)


..... Examiner
(Varun Taepaisitphongse, Ph.D.)


..... External Examiner
(Assistant Professor Worapon Kiatkittipong, D. Eng.)

ญาสุนันท์ วัฒนสุรวิทย์ : เซลล์แสงอาทิตย์ชนิดสีย้อมไวแสงที่มีชั้นอิเล็กโทรดชนิด $\text{Fe}_2\text{O}_3/\text{TiO}_2$, WO_3/TiO_2 หรือชนิด $\text{CeO}_2/\text{TiO}_2$. (DYE SENSITIZED SOLAR CELL WITH $\text{Fe}_2\text{O}_3/\text{TiO}_2$, WO_3/TiO_2 OR $\text{CeO}_2/\text{TiO}_2$ ELECTRODE LAYER)
 อ.ที่ปรึกษาวิทยานิพนธ์หลัก: อ.ดร.อัศววัต ศิริสุข, 78 หน้า.

ไทเทเนียมไดออกไซด์เป็นชั้นอิเล็กโทรดสำหรับเซลล์แสงอาทิตย์ชนิดสีย้อมไวแสงโดยมีการเตรียมชั้นฟิล์มด้วยการเคลือบไทเทเนียโซลซึ่งเตรียมด้วยวิธีโซลเจลด้วยเครื่องพ่นอัลตราโซนิก โดยงานวิจัยนี้จะศึกษาผลของอุณหภูมิในการเผา ความหนาของชั้นฟิล์ม และการเติมโลหะออกไซด์ชนิดต่าง ๆ ลงไปในชั้นไทเทเนียฟิล์มที่มีผลต่อประสิทธิภาพของเซลล์ จากการทดลองพบว่า การพ่นไทเทเนียมไดออกไซด์โซลที่ 250 รอบ วัดความหนาได้ประมาณ 5.05 ไมโครเมตร ที่อุณหภูมิในการเผา 400 องศาเซลเซียส จะให้ประสิทธิภาพของเซลล์แสงอาทิตย์ที่ดีที่สุด หลังจากนั้นชั้นฟิล์มไทเทเนียมไดออกไซด์ได้ถูกปรับปรุงโดยการเติมเฟอร์ริกออกไซด์ ทังสเตนออกไซด์ และซีเรียมออกไซด์ที่อัตราส่วนโดยน้ำหนักต่าง ๆ ด้วยวิธีโซลเจล จากการทดลองพบว่า การเติมโลหะออกไซด์ลงไปจะทำให้พื้นที่ผิวเพิ่มมากขึ้นนำไปสู่การปรับปรุงค่าของกระแสและประสิทธิภาพของเซลล์เมื่อทำการเปรียบเทียบกับเซลล์ที่มีเพียงแต่ไทเทเนียมไดออกไซด์ ยกเว้นในกรณีของการเติมเฟอร์ริกออกไซด์ซึ่งพบว่าประสิทธิภาพของเซลล์มีค่าลดลงเนื่องมาจากการที่เฟอร์ริกไอออนประพฤติตัวเป็นจุดศูนย์กลางในการเกิดการรวมตัวกันของอิเล็กตรอนที่ดีซึ่งพิจารณาจากค่าของกระแสและความต่างศักย์ และประสิทธิภาพของเซลล์จะลดลง เมื่อมีการเติมโลหะทังสเตนที่จำนวนรอบในการเคลือบมากกว่า 150 รอบ เซลล์ที่มีการเติมซีเรียมออกไซด์ลงไป 1% โดยน้ำหนักของซีเรียมออกไซด์ต่อไททาเนียมไดออกไซด์ที่ความหนา 250 รอบและอุณหภูมิในการเผา 400 องศาเซลเซียส พบว่าประสิทธิภาพของเซลล์แสงอาทิตย์จะดีที่สุดคือ 3.23%

ศูนย์วิทยทรัพยากร

จุฬาลงกรณ์มหาวิทยาลัย

ภาควิชา..... วิศวกรรมเคมี..... ลายมือชื่อนิสิต..... ญาสุนันท์
 สาขาวิชา..... วิศวกรรมเคมี..... ลายมือชื่อ อ.ที่ปรึกษาวิทยานิพนธ์หลัก.....
 ปีการศึกษา..... 2551.....

4970289521 : MAJOR CHEMICAL ENGINEERING

KEYWORDS : DYE SENSITIZED SOLAR CELL / SOL-GEL / TITANIUM DIOXIDE

YASUNUN WATTANASURAWIT: DYE SENSITIZED SOLAR CELL WITH $\text{Fe}_2\text{O}_3/\text{TiO}_2$, WO_3/TiO_2 OR $\text{CeO}_2/\text{TiO}_2$ ELECTRODE LAYER.

THESIS ADVISOR: AKAWAT SIRISUK, Ph.D. 78 pp.

A titanium dioxide electrode layer for a dye sensitized solar cell (DSSC) was prepared from ultrasonic spray coating of TiO_2 sol, which was synthesized via a sol-gel method. The effects of sintering temperature, film thickness, and modification of TiO_2 layer by another metal oxide on the efficiency of the dye sensitized solar cell were studied. The highest efficiency for pure TiO_2 electrode was obtained when the number of coats of TiO_2 layer was 250, corresponding to a thickness of ca. 5 μm , and a sintering temperature for TiO_2 layer of 400 °C. The preparation of the $\text{Fe}_2\text{O}_3/\text{TiO}_2$, WO_3/TiO_2 and $\text{CeO}_2/\text{TiO}_2$ electrode layers with different weight ratio was also based on sol-gel methods. The mixed metal oxides possessed larger specific surface areas than pure TiO_2 did. Large specific area brought about improvement on short-circuit photocurrent and solar energy conversion efficiency when compared to a cell that was fabricated by pure TiO_2 electrode, except the case of $\text{Fe}_2\text{O}_3/\text{TiO}_2$. $\text{Fe}_2\text{O}_3/\text{TiO}_2$ electrode gave rise to DSSC because Fe^{+3} acted as a recombination center for the photogenerated charge carriers, which was evident from decline in both I_{SC} and V_{OC} . The efficiency of the cell with WO_3/TiO_2 electrode was lower when number of TiO_2 coats exceeded 150. The cell that incorporated 1 wt% $\text{CeO}_2/\text{TiO}_2$ electrode with number of TiO_2 layers was 250, which was sintered at 400°C, produced the best solar energy conversion efficiency of 3.23%.

Department : Chemical Engineering..... Student's Signature *Signature*

Field of Study : Chemical Engineering..... Advisor's Signature *Signature*

Academic Year : 2008.....

ACKNOWLEDGEMENTS

This thesis would not have been possible to complete without the support of the following individuals. Firstly, I would like to express my greatest gratitude to my advisor, Dr. Akawat Sirisuk, for his invaluable guidance during the course of this work. And I am also very grateful to Associate Professor Sarawut Rimdusit, for his kind supervision over this thesis as the chairman, Dr. Varun Taepaisitphongse and Assistant Professor Worapon Kiatkittipong, from Faculty of Engineering and Industrial Technology, Silpakorn University as the members of the thesis committee.

The financial supports from Thailand Research Fund, Commission on Higher Education and Graduate School of Chulalongkorn University are also gratefully acknowledged.

I would like to acknowledge with appreciation to Professor Piyasan Praserttham for his kind suggestions without hesitation on my research.

Many thanks for kind suggestions and useful help to staffs of NECTEC at NSTDA for solar simulation (I-V tester) and many friends in the Center of Excellence on Catalysis and Catalytic Reaction Engineering who always provide the encouragement and assistance along the study. To the many others, not specifically named, who have provided me with support and encouragement, please be assured that I think of you.

Finally, I would like to dedicate this thesis to my parents, my brothers and sisters who always pay attention to me all the times, for suggestions and for listening to my complaints.

จุฬาลงกรณ์มหาวิทยาลัย

CONTENTS

	Page
ABSTRACT (THAI).....	Iv
ABSTRACT (ENGLISH).....	v
ACKNOWLEDGEMENTS.....	vi
CONTENTS.....	vii
LIST OF TABLES.....	x
LIST OF FIGURES.....	xii
CHAPTER	
I INTRODUCTION	1
II BACKGROUND INFORMATION	4
2.1 Operation principles and structure of DSSC.....	4
2.1.1 Cell structure.....	4
2.1.2 Operating Principles.....	5
2.2 Characteristics of the Photovoltaic Cell.....	7
2.2.1 Photocurrent density.....	7
2.2.2 Open circuit voltage.....	7
2.2.3 Fill factor.....	8
2.2.4 Efficiency.....	9
2.3 Performance of DSSC.....	10
2.4 State-of-the-art material and current development in DSSC.....	11
2.4.1 Dye sensitized.....	11
2.4.2 Electrolyst.....	13
2.4.3 Nanocrystalline titania dioxide film.....	13
2.5 Parameter of TiO ₂ electrode influence of overall efficiency of DSSC.....	14
2.5.1 Preparation method of TiO ₂	14
2.5.2 Thickness of TiO ₂ film.....	15
2.5.3 Sintering temperature of TiO ₂ film.....	16
2.5.4 Modification of TiO ₂	18

CHAPTER	Page
III EXPERIMENTAL	24
3.1 Preparation of TiO ₂ film and metal oxide dope TiO ₂ film.....	24
3.1.1 Preparation of TiO ₂ sol.....	24
3.1.2 Preparation of metal oxide dope TiO ₂ sol.....	24
3.1.2.1 Preparation of Fe ₂ O ₃ /TiO ₂ sol.....	25
3.1.2.2 Preparation of WO ₃ /TiO ₂ sol.....	25
3.1.2.3 Preparation of CeO ₂ /TiO ₂ sol.....	25
3.2 Preparation of dye sensitized solar cell components and the fabrication procedure.....	26
3.2.1 Transparent conducting glass.....	26
3.2.2 Dye.....	26
3.2.3 Electrolyte.....	27
3.2.4 Counter electrode.....	27
3.2.5 Working electrode	28
3.2.6 Fabrication of dye sensitized solar cell assembly.....	29
3.3. Physical and Electrochemical Characterization.....	30
3.3.1 X-ray diffractometry (XRD).....	30
3.3.2 Nitrogen physisorption.....	30
3.3.3 UV-Visible Absorption Spectroscopy (UV-Vis).....	30
3.3.4 Photoluminescence (PL).....	31
3.3.5 Inductively Coupled Plasma-Atomic Emission Spectroscopy (ICP-AES).....	31
3.3.6 Scanning electron microscope (SEM).....	31
3.3.7 Current-Voltage Tester (I-V Tester).....	32
IV RESULTS AND DISCUSSION	33
4.1 Effect of sintering temperature for TiO ₂ electrode layer.....	33
4.2 Effect of thickness of TiO ₂ film	40
4.3 Effect of modification of TiO ₂ electrode layer.....	44
4.3.1 Modification of TiO ₂ electrode layer by Fe ₂ O ₃	44
4.3.2 Modification of TiO ₂ electrode layer by adding WO ₃	49
4.3.3 Modification of TiO ₂ electrode layer by adding CeO ₂	55

CHAPTER	Page
V CONCLUSIONS AND RECOMMENDATIONS.....	59
5.1 Conclusions.....	59
5.2 Recommendations for future studies.....	60
REFERENCES.....	61
APPENDICES.....	65
APPENDIX A CALCULATION OF THE CRYSTALLITE SIZE.....	66
APPENDIX B CALCULATION OF WEIGHT FRACTION OF ANATASE, RUTILE AND BROOKITE PHASE.....	68
APPENDIX C DETERMINATION OF THE AMOUNT OF DYE ABSORBED ON TITANIA SURFACE.....	70
APPENDIX D CALCULATION OF RESULT OF ICP-OES.....	71
APPENDIX E DATA OF THE ELECTROCHEMICAL PROPERTIES OF DYE SENSITIZED SOLAR CELL.....	72
APPENDIX F LIST OF PUBLICATIONS.....	77
VITA.....	78

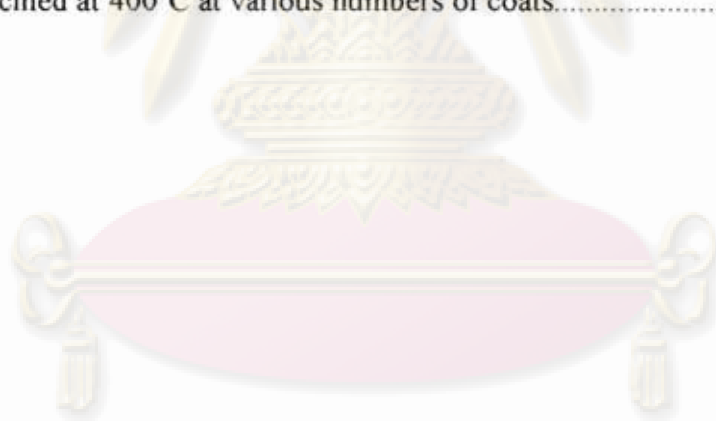


คุรุณย์วิทยทรรพยากร
จุฬาลงกรณ์มหาวิทยาลัย

LIST OF TABLES

Table	Page
2.1 Efficiency of DSSC with various device sizes.....	10
4.1 Crystal size, surface area and weight fraction of anatase, rutile and brookite phase of TiO ₂ powders sintered at various temperatures for 2 h.....	34
4.2 Electrochemical properties of DSSC with TiO ₂ electrode calcined at various temperature, the thickness of TiO ₂ was about 1.74 μm.....	39
4.3 Electrochemical properties of dye sensitized solar cells of TiO ₂ electrode calcined at 400°C with various thicknesses.....	42
4.4 Crystal size, surface area and weight fraction of anatase, rutile and brookite phase of Fe ₂ O ₃ /TiO ₂ powders sintered at 400°C for 2 h.....	45
4.5 Electrochemical properties of dye sensitized solar cells of Fe ₂ O ₃ /TiO ₂ electrode calcined at 400°C with number of coat was 100.....	47
4.6 Electrochemical properties of dye sensitized solar cells of 0.25 % wt Fe ₂ O ₃ /TiO ₂ electrode calcined at 400°C at various numbers of coats....	48
4.7 Crystal size, surface area and weight fraction of anatase, rutile and brookite phase of WO ₃ /TiO ₂ powders sintered at 400°C for 2 h.....	50
4.8 Crystal size, Surface area and weight fraction of anatase, rutile and brookite phase of CeO ₂ /TiO ₂ powders sintered at 400°C for 2 h.....	56
E.1 The electrochemical properties of TiO ₂ electrode calcined at 300°C with various numbers of coats.....	72
E.2 The electrochemical properties of TiO ₂ electrode calcined at 400°C with various numbers of coats.....	72
E.3 The electrochemical properties of TiO ₂ electrode calcined at 500°C with various numbers of coats.....	73
E.4 The electrochemical properties of TiO ₂ electrode calcined at 600°C with various numbers of coats.....	73
E.5 The electrochemical properties of 0.25 % wt Fe ₂ O ₃ /TiO ₂ electrode calcined at 400°C at various numbers of coats.....	73

Table	Page
E.6 The electrochemical properties of 1.0 % wt Fe ₂ O ₃ /TiO ₂ electrode calcined at 400°C at various numbers of coats.....	74
E.7 The electrochemical properties of 2.0 % wt Fe ₂ O ₃ /TiO ₂ electrode calcined at 400°C at various numbers of coats.....	74
E.8 The electrochemical properties of 0.25 % wt WO ₃ /TiO ₂ electrode calcined at 400°C at various numbers of coats.....	74
E.9 The electrochemical properties of 1.0 % wt WO ₃ /TiO ₂ electrode calcined at 400°C at various numbers of coats.....	75
E.10 The electrochemical properties of 2.0 % wt WO ₃ /TiO ₂ electrode calcined at 400°C at various numbers of coats.....	75
E.11 The electrochemical properties of 0.25 % wt CeO ₂ /TiO ₂ electrode calcined at 400°C at various numbers of coats.....	75
E.12 The electrochemical properties of 1.0 % wt CeO ₂ /TiO ₂ electrode calcined at 400°C at various numbers of coats.....	76
E.13 The electrochemical properties of 2.0 % wt CeO ₂ /TiO ₂ electrode calcined at 400°C at various numbers of coats.....	76



ศูนย์วิจัยทรัพยากร
จุฬาลงกรณ์มหาวิทยาลัย

LIST OF FIGURES

Figure		Page
2.1	Structure of dye sensitized solar cell.....	5
2.2	Operation principle of DSSC.....	6
2.3	I-V characteristic of an illuminated solar cell.....	8
2.4	Comparison of percentage of power between titania and silicon cells as a function of temperature.....	11
2.5	The structure of commercial dyes used in DSSC.....	12
2.6	Anchored of N3 dye on a TiO ₂ particle by ester linkage.....	12
2.7	I-V characteristics of P25 (a) multiple coats, (b) 1 coat, (c) 2 coats, (d) 3 coats and (e) 4 coats.....	16
2.8	Resistivity of SnO ₂ /ITO conducting glass annealed at various temperatures for 1 h.....	17
2.9	I-V characteristics of anatase and rutile films.....	18
2.10	The comparison I-V characteristic of pure TiO ₂ and mixed metal oxides (ZrO ₂ 5%+TiO ₂ 95%).....	20
2.11	Relation between of overall efficiency of cell and oxide composition.....	20
2.12	PL spectra of TiO ₂ nanoparticles with the excitation wavelength at 300 nm.....	21
2.13	PL spectra of Ce doped TiO ₂ at the excitation wavelength of 300 nm.....	22
2.14	PL spectra of W-doped TiO ₂ at the excitation wavelength of 325 nm.....	23
2.15	PL spectra of La doped TiO ₂ at the excitation wavelength of 300 nm.....	23
3.1	Show counter electrode before sputtering.....	27
3.2	Show anode electrode before spray coating.....	28
3.3	Cross-section of assembled dye solar cell showing sealing rim.....	29
3.4	Fabrication of dye sensitized solar cell assembly for testing.....	29
4.1	XRD patterns of TiO ₂ powders sintered at different temperature.....	34
4.2	SEM images of TiO ₂ powders calcined at different temperature.....	35

Figure	Page
4.3 Relationship between concentrations of dye and sintering temperature with 100 coats of TiO ₂ electrodes layer.....	37
4.4 FTIR spectra of TiO ₂ calcined at different temperatures.....	37
4.5 PL spectra of TiO ₂ at calcined at different temperature.....	38
4.6 Efficiency of DSSC of TiO ₂ at calcined at different temperature.....	40
4.7 Relationship between concentrations of dye with various thicknesses of TiO ₂ film.....	41
4.8 Efficiency of DSSC as a film thickness of TiO ₂ for the electrode.....	42
4.9 Relationship between concentrations of dye, sintering temperature (°C) and number of coat of TiO ₂ electrode.....	43
4.10 Efficiency of DSSC as a film thickness and sintering temperature of TiO ₂ electrode.....	43
4.11 XRD patterns of Fe ₂ O ₃ /TiO ₂ powders at various percentage of Fe/Ti.....	45
4.12 Relationship between concentrations of dye with various contents of Fe/Ti at different of number of coat of electrode.....	46
4.13 PL spectra of Fe ₂ O ₃ /TiO ₂ at various contents.....	47
4.14 Efficiencies of dye sensitized solar cells of Fe ₂ O ₃ /TiO ₂ electrode calcined at 400°C at various number of coat and the contents of Fe/Ti.....	49
4.15 XRD patterns of WO ₃ /TiO ₂ powders at various contents of W/Ti.....	50
4.16 Relationship between concentrations of dye with various contents of W/Ti at different of number of coat of electrode.....	51
4.17 PL spectra of WO ₃ /TiO ₂ at various contents.....	52
4.18 Efficiencies of dye sensitized solar cells of WO ₃ /TiO ₂ electrode calcined at 400°C at various number of coat and the contents of W/Ti.....	53
4.19 The density of current (I _{SC}) of cell of WO ₃ /TiO ₂ electrode calcined at 400°C at various number of coat and the contents of W/Ti.....	54
4.20 The open circuit voltage of WO ₃ /TiO ₂ electrode calcined at 400°C at various number of coat and the contents of W/Ti.....	55
4.21 XRD patterns of CeO ₂ /TiO ₂ powders at various percentage of Ce/Ti.....	56

Figure	Page
4.22 Relationship between concentrations of dye with various contents of Ce/Ti at different of number of coat of electrode.....	57
4.23 PL spectra of CeO ₂ /TiO ₂ at various contents.....	58
4.24 Efficiencies of dye sensitized solar cells of CeO ₂ /TiO ₂ electrode calcined at 400°C at various number of coat and the contents of Ce/Ti.....	59
A.1 The (101) diffraction peak of titania for calculation of the crystallite size.....	67
C.1 The calibration curve of the concentration of dye absorbed on titania.	70



ศูนย์วิทยทรัพยากร
จุฬาลงกรณ์มหาวิทยาลัย

CHAPTER I

INTRODUCTION

A dye sensitized solar cell (DSSC) is one type of photoelectrochemical cell. The cell is a device that converts solar energy into electrical energy by photovoltaic effect. The mechanism of this solar cell is similar to the photosynthesis process in plant. Dye sensitized solar cell was invented by Michael Grätzel and Brian O' Regan known as Grätzel cells (O'Regan and Grätzel, 1991). The DSSC is easy to prepare, inexpensive to produce and friendly to the environment. The voltage of the cell is significantly less sensitive to a variation in light intensity than that of conventional solar cells, thereby making this type of solar cells interesting for photovoltaic production.

The DSSC mainly consists of light sensitive dyes, a dye adsorber (TiO_2 , a wide band gap semiconductor), an electrolyte, front and back electrodes made of transparent conducting oxide. Under light irradiation, photo-excited electrons in the adsorbed dyes are injected into the conduction band of TiO_2 . After that, the electrons are collected by front electrode and supplied to external load. Then the dye molecules are electrically reduced to their initial states by electrons transferred from redox couple in the electrolyte. The oxidized ions in the electrolyte diffuse to the back electrode to receive electrons and finish the cycle.

TiO_2 have been used as a working electrode for DSSC because it can produce a higher efficiency than any other metal oxide. However, as reported, the best TiO_2 solar cell efficiency is around 11.2% (Chiba et al., 2006). In general, electrodes with high surface area are of great significance since a higher amount of dye adsorbed on an electrode corresponds to a higher current density acquired. To improve energy conversion efficiency, TiO_2 electrodes with large surface areas have been investigated extensively as a key role for dye sensitized solar cells (Yoshikawa et al., 2006).

The morphology, particle size, and preparation methods of the TiO_2 photoelectrode play a key role in photoelectric conversion efficiency of DSSC (Lee et al., 2007). The standard requirements of TiO_2 electrode layer for DSSC include pure anatase phase, high surface area for adsorption of dye molecules and nanoparticle network for better electronic percolation (Karthikeyan et al., 2006).

For example, the activity of TiO_2 nanoparticles is higher than that of a commercial photocatalyst (P25) because of its high surface area, which allows efficient adsorption of dye molecules, and diffusion coefficient of electron in TiO_2 nanocrystal are higher value, hence a lower chance of recombination with increasing particle sizes (Zhao et al., 2008).

Nanocrystalline films containing 30% rutile have smaller specific than anatase-based cell so lesser amount of dye can be adsorbed on rutile. Moreover diffusion of electron in rutile layer is slower than in anatase layer because of different in extent of interparticle connectivity related with the particle packing density (Park et al., 2000).

Several research groups have attempted to improve the properties of the TiO_2 electrode by using a bi-layer technique to modify the structure of TiO_2 with GeO_2 , ZrO_2 , Al_2O_3 , MgO , SiO_2 and ZnO (Thavasi et al., 2008). For example, the addition of ZrO_2 in to TiO_2 leads to a have higher surface area and the ability to adsorb dye is increased, thereby with increasing the open-circuit photo voltage of dye sensitized solar cells (Kitiyanan et al., 2005 and Yoshikawa et al., 2006).

Therefore, this work focused the study on the effects of sintering temperature and thickness of TiO_2 electrode layer, and the addition effect of Fe_2O_3 , WO_3 , or CeO_2 addition on the properties and efficiency of the dye sensitized solar cell. TiO_2 , $\text{Fe}_2\text{O}_3/\text{TiO}_2$, WO_3/TiO_2 and $\text{CeO}_2/\text{TiO}_2$ sol are prepared via sol gel method. The photovoltaic properties of dye sensitized solar cell is determined using the I-V tester.

ศูนย์วิจัยทรัพยากร
จุฬาลงกรณ์มหาวิทยาลัย

Objective

1. To study the effect of the efficiency of a dye sensitized solar cell (DSSC) by adding Fe_2O_3 , WO_3 and CeO_2 to TiO_2 electrode layer.
2. To study the influence of sintering temperature and thickness of electrode layer on the efficiency of the dye sensitized solar cell.

The thesis is arranged as follows:

Chapter I presented the introduction of this study.

Chapter II presented the background information related to this research such as basic principles of dye sensitized solar cell, basic information about TiO_2 and preparation of TiO_2 electrode layer, and also literature reviews of previous works related to this research.

Chapter III described the synthesis of the TiO_2 sol and modified TiO_2 sol via sol-gel methods, the preparation of TiO_2 film, the fabrication procedure of DSSC and characterization techniques used in this study.

Chapter IV presented and discuss experimental results.

In the last chapter, Chapter V, the overall conclusions and recommendations for the future studies were given.

ศูนย์วิทยทรัพยากร
จุฬาลงกรณ์มหาวิทยาลัย

CHAPTER II

BACKGROUND INFORMATION

2. Dye sensitized Solar Cell (DSSC)

Dye sensitized solar cell (DSSC) had historically originated in the 19th century (Jenny Nelson, 2004). It was used in photovoltaic rather unsuccessful until the early 1990s. Grätzel and coworkers had developed the so-called dye sensitized nanostructure solar cell or the Grätzel cell, with the efficiency conversion exceeding 7% in 1991 by combination of nanostructure electrode and efficiency charge injection dye (Baumann et al., 2004). The cell is an alternative solar cell technology based on photoelectrochemical mechanism. The cell resembles photosynthesis in plant. Therefore, this system has been described in terms of artificial photosynthesis such as chlorophyll in plants as same as monolayer of dye molecules (sensitizers) adsorbs the incident light, giving rise to the generation of positive and negative charge carriers (Lenzmann and Kroon, 2007). Recently, the efficiency of this cell was raised up to 11.2% (Chiba et al., 2006).

2.1 Operation Principles and Structure of DSSC

2.1.1 Cell Structure

The DSSC mainly consists of adsorbed complex dye, SnO₂ conductor, a nanocrystalline tiania layers, an electrolyte solution and a platinum layers (see Figure 2.1). The photoelectrode comprises of metal oxide (wide band-gap semiconductor film), e.g., TiO₂, deposited on a transparent oxide conducting glass. A ruthenium complex dye is dye sensitizer which is adsorbed onto the semiconductor film. The counter electrode is made up of a catalyst (usually platinum) attached to another piece of conducting glass. A redox pair consisting of Iodide (I^-)/(I_3^-) acts as an electrolyte in this cell.

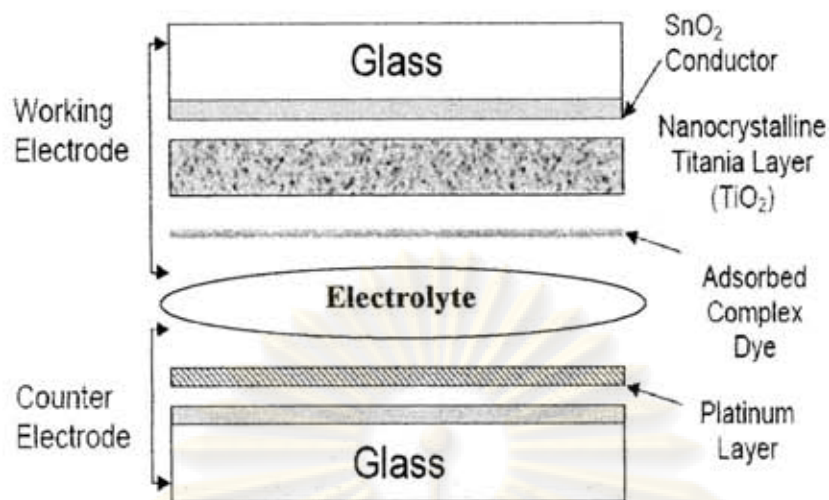


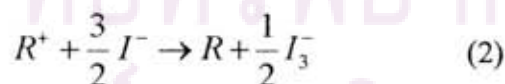
Figure 2.1 Structure of dye sensitized solar cell (Phani et al., 2001)

2.1.2 Operating Principles

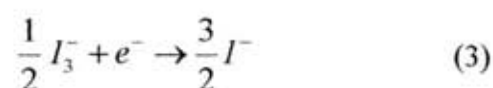
In detail, the operation of dye sensitized solar cell can be described in schematic structure of DSSC (Figure 2.2), leading to the direct conversion of sunlight to electrical energy. Firstly, upon light adsorption the dye molecules is excited from their ground state (R) to an excited state (R^*).



The dye injects an electron into the conduction band (CB) of semi-conductor layer (TiO_2), leaving an oxidized dye molecule (R^+). The electron donor present in the electrolyte (I^-) reduces the oxidized dye (R^+) back to its ground state (R). This leads to the regeneration of the charge neutral state of the sensitizer.



Then the electrons pass through to the external circuit to arrive at the conventional electrode where they undergo the reverse redox reaction.



There are a number of undesired pathways in this process. The electrons in the conduction band can reduce the oxidized dye (R^+) or can regenerate the redox couple.



One of the major limiting factors of these cells is the back electron transfer of these undesired reactions. The high back electron transfer is due to the fact that TiO_2 lacks a depletion layer between the working electrode and electrolyte filling (Kalyanasundaram et al., 1998 and Kartini, 2004).

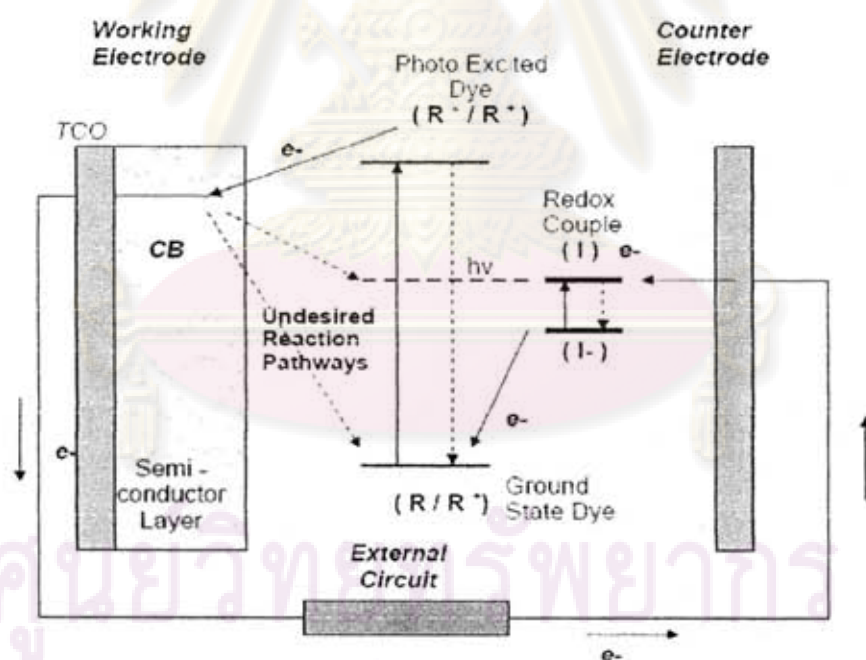


Figure 2.2 Operation principle of DSSC (Kalyanasundaram et al., 1998)

2.2 Characteristics of the Photovoltaic Cell (Jenny Nelson, 2004)

There are four key characteristic that are used to describe efficiency of DSSC, namely, short-circuit current (I_{SC}); the maximum current at zero voltage, open-circuit voltage (V_{OC}); the maximum voltage at zero current, fill factor (FF) and η (efficiency).

2.2.1 Photocurrent density

The photocurrent generated by a solar cell under illumination at short circuit is dependent on the incident light so call the photocurrent density, I_{SC} . It depends on the adsorption coefficient of the solar cell material, the efficiency of charge separation and the efficiency of charge collection in the device but does not depend on the incident spectrum. It is therefore a key quantity in describing solar cell performance under different conditions.

2.2.2 Open circuit voltage

The open-circuit voltage or V_{OC} , It is the maximum voltage from a solar cell with occurs at zero current. The open-circuit voltage corresponds to the amount of forward bias on the solar cell due to the bias of the solar cell junction with the light-generated current. The equation for V_{OC} is found by setting the net current equal to zero see in equation below.

$$V_{oc} = \frac{kT}{q} \ln\left(\frac{I_{sc}}{I_0} + 1\right) \quad (6)$$

Where $\frac{kT}{q}$ is the thermal voltage

I_0 = saturation current

I_L = light generated current

The equation shows that V_{OC} depends on the saturation current of the solar cell and the light-generated current. While I_{sc} typically has a small variation, the key effect is the saturation current. The saturation current, I_0 depends on recombination in the solar cell. Open-circuit voltage is then a measure of the amount of recombination in the device. The open-circuit voltage is shown on the I-V curve in Figure 2.3.

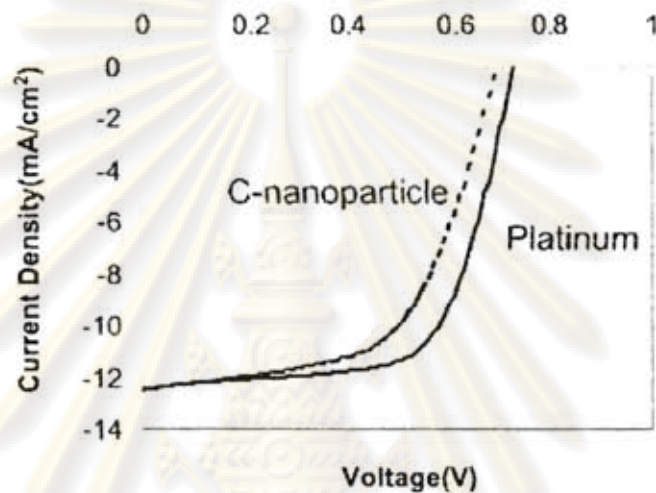


Figure 2.3 I-V characteristic of an illuminated solar cell (Prakash Joshi et al, 2008)

2.2.3 Fill factor

All of these should be defined for particular illumination conditions. The cell power density is given by

$$P = IV \quad (7)$$

Where

P = the power (watt or W)

I = the current (ampere or A)

V = potential difference (volt or V)

This occurs at some voltage V_{mp} with a corresponding current density I_{mp} , shown in Figure 2.3. The maximum power output of a cell is graphically given by the largest rectangle that can be filled under the I-V curve. The optimum load thus has sheet resistance given by V_{mp}/I_{mp} .

The fill factor is defined as the ratio

$$FF = \frac{I_{mp} V_{mp}}{I_{sc} V_{oc}} \quad (8)$$

Where

I_{mp} = the current at maximum power

V_{mp} = potential difference at maximum power

FF = fill factor

I_{sc} = the short-circuit current

V_{oc} = the open-circuit voltage

2.2.4 Efficiency

The efficiency η of the cell is the power density delivered at operating point as a fraction of the incident light power density, P_s ,

$$\eta = \frac{I_{mp} V_{mp}}{P_s} \quad (9)$$

Efficiency is related to I_{sc} and V_{oc} using FF,

$$\eta = \frac{I_{sc} V_{oc} FF}{P_s} \quad (10)$$

Where

η = efficiency of solar cell

P_s = power of light source

2.3 Performance of DSSC

In 2007, the best device has a size of less than 1 cm² (see in Table 2.1), with efficiency of 11.2% under standard test conditions (1000W/m², AM1.5, 298K). The size is small device (area is smaller) with higher efficiency have been reported (Lenzmann and Kroon, 2007).

Table 2.1 Efficiency of DSSC with various device sizes (Lenzmann and Kroon, 2007)

Dye	Surface area (cm ²)	Efficiency (%)	V _{OC} (Volt)	I _{sc} (mA/cm ²)	FF (%)
N-719	< 1	11.2	0.84	17.73	74
N-749	0.219	11.1	0.736	20.9	72
N-749	1.004	10.4	0.72	21.8	65
N719	1.31	10.1	0.72	17.0	72
N-3	2.36	8.2	0.82	15.8	71

DSSC has performance advantage over other solar cell, which include the ability to perform well in low light and shade, and to improve in performance with increasing temperature (see Figure 2.4) under standard conditions (1000W/m², AM 1.5 and 25⁰C) (Phani et al., 2001).

ศูนย์วิทยทรัพยากร
จุฬาลงกรณ์มหาวิทยาลัย

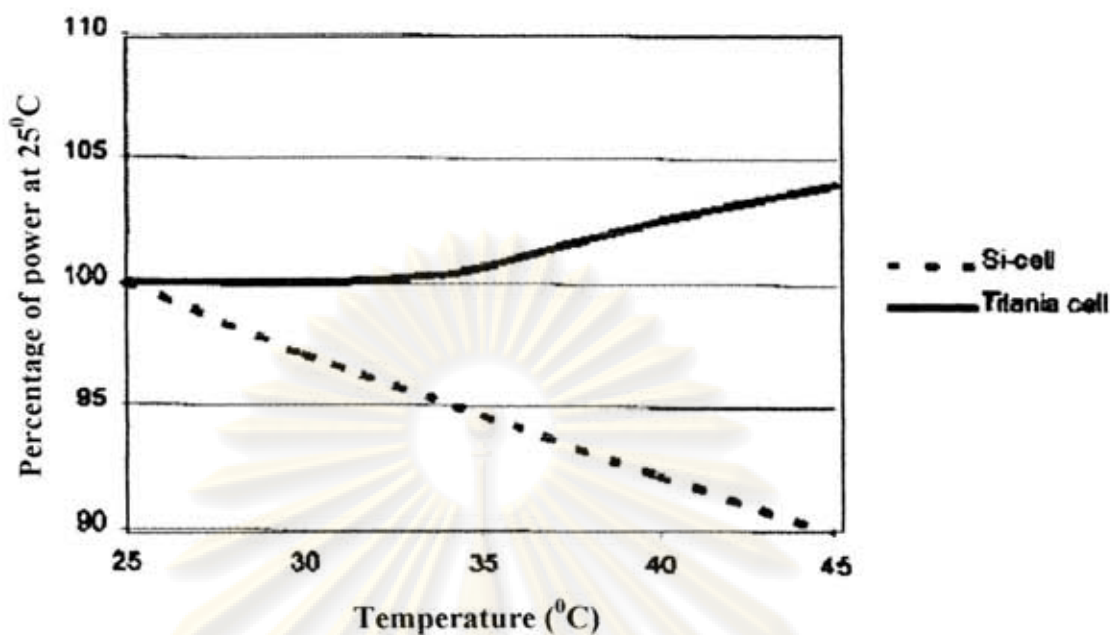


Figure 2.4 Comparison of percentage of power between titania and silicon cells as function of temperature (Phani et al., 2001)

2.4 State-of-the-art material and current development in DSSC

The key of efficiency in DSSC is materials of device, has active, the standard requirements of DSSC, such as dye have enhanced molar adsorption coefficients are attractive with TiO_2 layer. TiO_2 electrode have high surface area for adsorption of dye molecules and nanoparticle network for better electronic percolation (Karthikeyan et al., 2006) etc.

2.4.1 Dye sensitized

A ruthenium complex dye is dye sensitizer which is adsorbed onto the semiconductor film. Three dyes can be considered the backbone of currently in DSSC, dye consisted of ruthenium based metal organic complexes. The commercial of dyes is a widely used in DSSC. The dyes have three types are N3, N-749 and Z-907 (see Figurer 2.5).

In 1993, N3 dye is a widely used in DSSC where have been composed of two thiocyanate ligands with additional carboxylate group as anchoring sites on a TiO_2

particle by ester linkage seen in Figure 2.6. It is still widely employed as a reference. In 2001, to improve the dye, so call black dye, have a higher short circuit current.

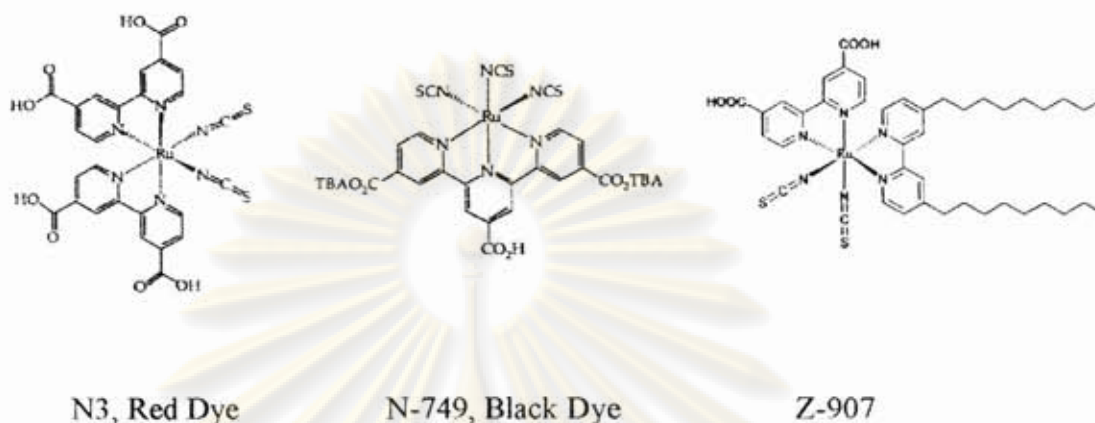


Figure 2.5 The structure of commercial dyes used in DSSC
(Lenzmann and Kroon, 2007)

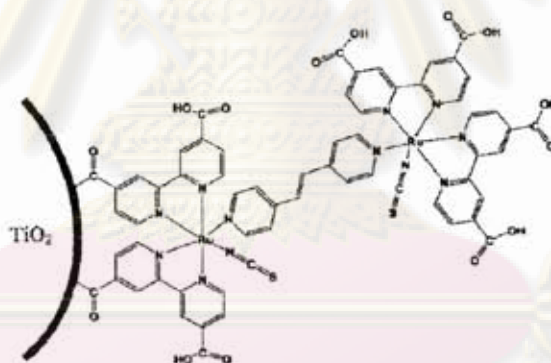


Figure 2.6 Anchored of N3 dye on a TiO_2 particle by ester linkage.
(Jang et al., 2005)

Dyes employed in highly efficiency in DSSC have suitable properties, have enhanced molar adsorption coefficients are attractive with TiO_2 layer, the energy level of the ground/excited state, the rate constant of charge injection/recombination and the stated of oxidization is stable (Lenzmann and Kroon, 2007).

Modification of the dye is one of the strategies to improve the performance of DSSC, for example, attaching hydrophobic chains to the pyridine rings in N3 dye, increasing the open-circuit voltage (V_{oc}) (Jang et al., 2005).

2.4.2 Electrolyte

A liquid electrolyte based on acetonitrile has a low viscosity, volatile solvent and using comparatively low iodine concentration. The goal improves the efficiency by additive into electrolytes, which to reduce dark current, improving the V_{OC} of the DSSC.

Several research groups use of ionic liquids instead of organic solvents in liquid electrolytes which has high stability, negligible vapor pressure and non-flammability as well as excellent environmental compatibility. On the other hand, overall power conversion efficiencies obtained with ionic liquids are lower than with organic solvent electrolytes (Lenzmann and Kroon, 2007).

2.4.3 Nanocrystalline titania dioxide film

Metal oxide as the material of choice for DSSC, It has been used as a working electrode because it has a wide band gap energy such as TiO_2 , ZnO , $SrTiO_3$ and Nb_2O_5 (Lenzmann and Kroon, 2007). However, as reported, the best TiO_2 solar cell efficiency is around 11.2 % (Chiba et al., 2006).

Titanium dioxide (TiO_2) is an n-type wide band gap semiconductor (band gap: 3.2 eV) which is the most commonly used working electrode in the DSSC. Titania has three main crystalline phases: anatase, which shows a higher photocatalytic activity than the other types of titanium dioxide and is desirable for DSSC; rutile, which tends to be more stable at higher temperatures; and brookite, which is usually found only in minerals.

The performance of DSSC is related to the characteristics of the semiconductor layer (TiO_2 film) such as the morphology, particle size, optical properties and preparation methods of the TiO_2 photoelectrode which play a key role in photoelectric conversion efficiency of DSSC (Lee et al., 2007).

The standard requirements of TiO_2 electrode layer for DSSC such as pure anatase phase, high surface area for adsorption of dye molecules (Karthikeyan et al., 2006), the pore size distribution, porosity, and pore structure allows the liquid electrolyte to fill all pores of the film and the nanocomposite geometry required contact of every dye molecule to both the TiO_2 as well as the electrolyte phase.

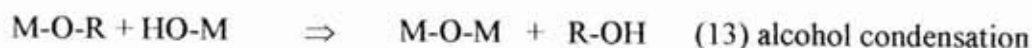
The morphology of TiO₂ electrode layer play a significant role in overall efficiency of DSSC because of influences of the different of preparation method, composition, sintering temperature and thickness of film of the TiO₂ electrode on overall efficiency of DSSC.

2.5 Parameter of TiO₂ electrode influence of overall efficiency of DSSC

2.5.1 Preparation method of TiO₂

The TiO₂ film prepared three different method are sol-gel (FMF), thermal (P-25), and colloidal-microwave processes (CMP), the difference in the preparation led to different surface areas, pore sizes and morphologies of the mesoporous films. FMF-TiO₂ displayed the highest efficiency and the highest incident photon to current conversion (IPCE) in DSSC because it contained pure anatase phase and its surface area and pore structure is optimal for efficient functioning of DSSC. P-25 films possessed pore structural and morphological features similar to FMF films. However, the efficiency of P-25 films was lower than that of FMF-TiO₂ due to the presence of small amount of rutile phase. Although CMP films possessed large surface area, its pore diameter was smaller together with the presence of agglomerates and macropores, leading to lower efficiency. Therefore, the optimal pore and morphological structures were necessary for efficient functioning of solid-state dye sensitized solar cell (Karthikeyan et al., 2006).

The sol-gel method occurs in liquid solution of organometallic precursors such as tetraethyl orthosilicate, zirconium propoxide and titanium isopropoxide, which, by means of hydrolysis and condensation reaction, lead to the formation of sol (Su et al., 2004)



2.5.2 Thickness of TiO₂ film

The commonly of coating TiO₂ on a glass have difference method are doctor blade, spray coating, spin coating, vapor deposition, screen printing and reactive sputtering. Halme and coworkers (2006) studied the spray deposition of TiO₂ powder suspension at the room temperature compression as a method to prepare nanostructured TiO₂ films for dye sensitized solar cells. Relatively good solar cell performance of a light intensity of 2.8% at 100 mW/cm² was achieved with the method. The critical point in the spray deposition method was the successful control of the evaporation rate of the suspension liquid with respect to the deposition rate. This preserved the agglomerated nature of the deposited film originating from the spray droplets and prevented macroscopic cracking and flaking of the film during drying.

Film thickness is one of the important factors. Thickness affects the performance of the cells because the injected electrons have to be transported across a large number of colloidal particles and grain boundaries. One study has shown that film thickness increased with the short-circuit photocurrent (I_{sc}) increased because of because of increasing the absorption of dye on TiO₂ surface (Kang et al., 2004). Also, Kartini and Lu shown that the efficiency of the cells increases with number of coat increases (see Figure 2.7).

However the thickness increases the chance of recombination should increase. Therefore, there exists an optimum film thickness to obtain a maximum photo-voltage and fill factor (Kalyanasundaram et al., 1998).

These properties of films can be controlled using recent advances in colloid chemistry. Advances in precursor chemistry, hydrothermal growth temperatures, binder addition and sintering conditions have also contributed to the optimization of certain properties of the films (Brammer et al., 2004).

จุฬาลงกรณ์มหาวิทยาลัย

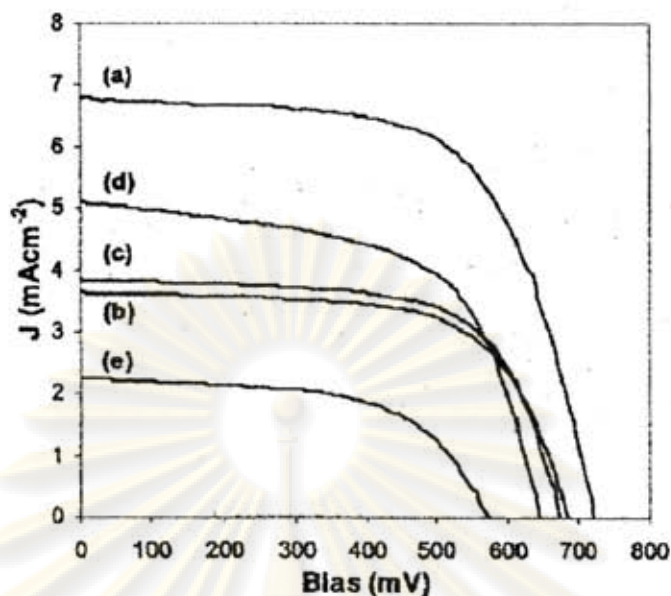


Figure 2.7 I-V characteristics of P25 (a) multiple coats, (b) 1 coat, (c) 2 coats, (d) 3 coats and (e) 4 coats (Kartini and Lu, 2004)

2.5.3 Sintering temperature of TiO₂ film

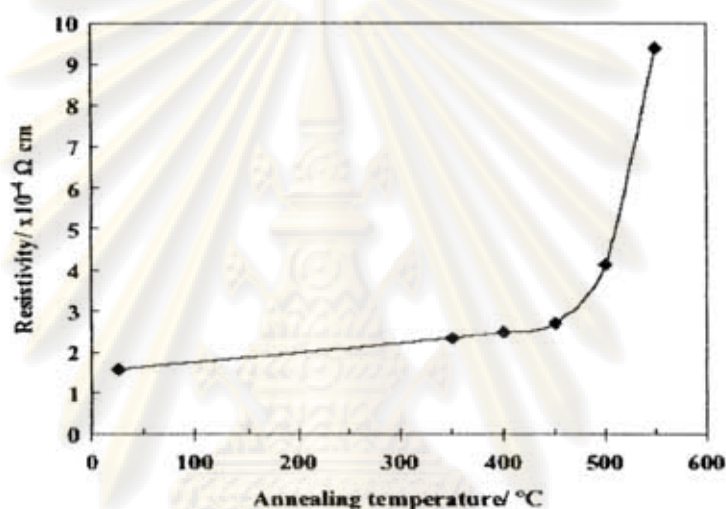
In general, sintering temperature and time affect photocurrent-voltage characteristic because of the change of crystalline size, size of pore, surface area and grain size of titania. Beside, sintering conditions affect the conductivity and light transmittance of the substrate which works as a current collector and properties. The resistivity of SnO₂/ITO was increased after thermal treatment at high (see Figure 2.8) (Ngamsinlapasathian et al., 2005).

Pore diameter and surface area of TiO₂ were very important in determining the cell efficiency with an increase in hydrothermal temperature, the pore diameter increased linearly. However, the surface area showed the reverse effect (Huang et al., 2006). TiO₂ have high surface area which allows efficient adsorption of dye molecules and diffusion coefficients of electron in TiO₂ nanocrystalline have a higher while a lower chance of recombination with increasing the particle sizes (Zhao et al., 2008).

Beside, the power conversion efficiency increasing with the increased in sintering temperature and becomes saturated at 400–500°C. Both the electron lifetime and the electron diffusion coefficient increase with the increase in sintering temperature. However, the evolution of rutile TiO₂ which possesses larger size, less

surface area cause the dye adsorption and slower electron diffusion rate due to low efficiency (Lee et al., 2007).

Nanocrystalline rutile films (rutile-base cell about 30%) have surface area per unit volume less than anatase-base cell so amount of dye adsorbed lesser than. Thus current density of anatase phase more than rutile phase (see Figure 2.9). Beside diffusion of electron in rutile layer is slower than in anatase layer because of different in extent of interparticle connectivity related with the particle packing density (Park et al., 2000).



Figurer 2.8 Resistivity of SnO_2/ITO conducting glass annealed at various temperatures for 1 h (Ngamsinlapasathian et al., 2005)

ศูนย์วิทยทรัพยากร
จุฬาลงกรณ์มหาวิทยาลัย

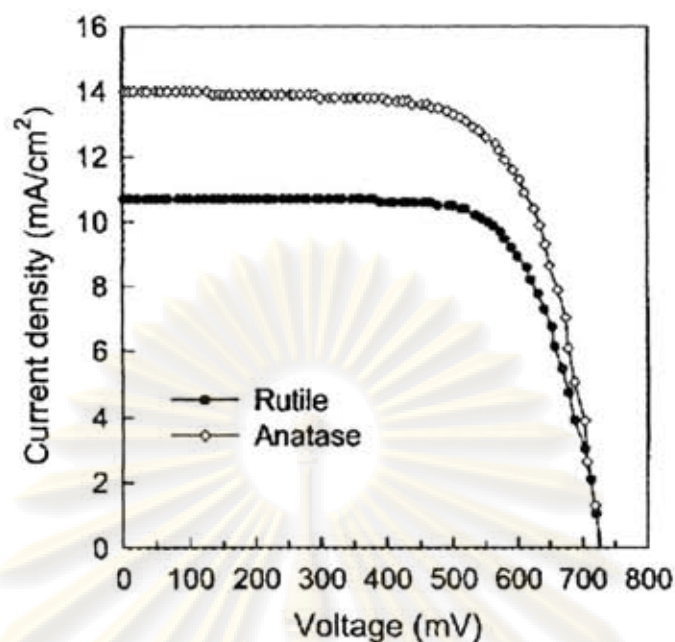


Figure 2.9 I-V characteristics of anatase and rutile films (Park et al., 2000)

2.5.4 Modification of TiO₂

Mixed-metal oxides play a very important role in chemistry, physics and materials science. Recently, there has been interest in phenomena associated with the deposition of oxide nanoparticles on the surface of a second oxide. In principle, the combination of two metals in an oxide matrix can produce materials with novel structural and/or electronic properties (Park et al., 2009).

The role of added metal was based on optical properties and morphology such as the crystal growth inhibitor, which leads to smaller grain size with high surface area. It shows that the higher efficiency when TiO₂ based mixed metal oxides (Yoshikawa et al., 2006).

Several research groups attempted to improve the properties of the TiO₂ electrode by addition of metal oxide to modify the structure of TiO₂ such as ZrO₂ and GeO₂ or dope metal ion such as Al and W on to TiO₂, for example the addition of ZrO₂ into TiO₂ has higher surface area than the pure component. It could be achieved and the ability to adsorb dye was increased with increasing the open-circuit photo voltage of dye sensitized solar cells (see Figure 2.10) (Kitiyanan et al., 2005 and Yoshikawa et al., 2006).

The effects of different metal oxide in to TiO_2 play a significant role in overall efficiency of DSSC. Kitiyanan and coworkers prepared TiO_2 , GeO_2 , and $\text{TiO}_2/\text{GeO}_2$ mixed oxide with different Ti/Ge ratio based on a sol-gel method with surfactant-assisted mechanism. When an amount of GeO_2 content is less than 10 mol%, the added germanium could serve as a crystal growth inhibitor that can cause a higher surface area, which resulted in the higher amount of adsorbed dye concentration. The electrodes fabricated at 10 mole% of $\text{TiO}_2/\text{GeO}_2$ gave significant highest efficiency of DSSC when compared to cell that fabricated by pure TiO_2 electrode but percentage of GeO_2 up to 20 mole% found that efficiency decreased because of decreasing of surface area (see Figure 2.11)(Kitiyanan et al., 2006).

Beside, Ko and coworker study TiO_2 doped with metal ion are Al and W by a sol-gel method. They found that Al-doped TiO_2 electrodes increased open-circuit voltage (V_{OC}), but reduced short-circuit current (I_{SC}). On the other hand W-doped TiO_2 had an opposite effect. Dye sensitized solar cell characteristics fabricated with doped TiO_2 were remarkably better than those with undoped TiO_2 . The role of the dopant was based on two effects: powder morphology and defect content such as Ti^{3+} . These modifications led to significant changes in powder aggregation, charge transfer kinetics, and dye adsorption characteristics. The highest efficiency was observed in TiO_2 that was doped with both Al and W (Ko et al., 2005).

However, the use of mixed metal oxide as an electrode was an alternative approach to enhance the efficiency of DSSC.

ศูนย์วิจัยทรัพยากร
จุฬาลงกรณ์มหาวิทยาลัย

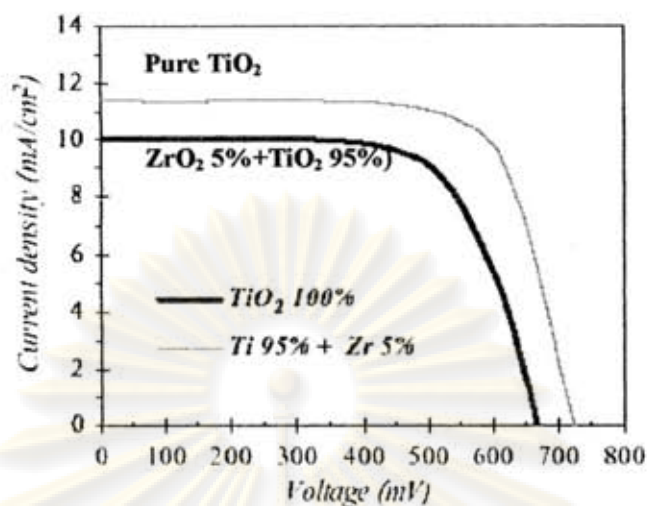


Figure 2.10 The comparison I-V characteristic of pure TiO₂ and mixed metal oxides (ZrO₂ 5%+TiO₂ 95%) (Kitiyanan et al., 2005)

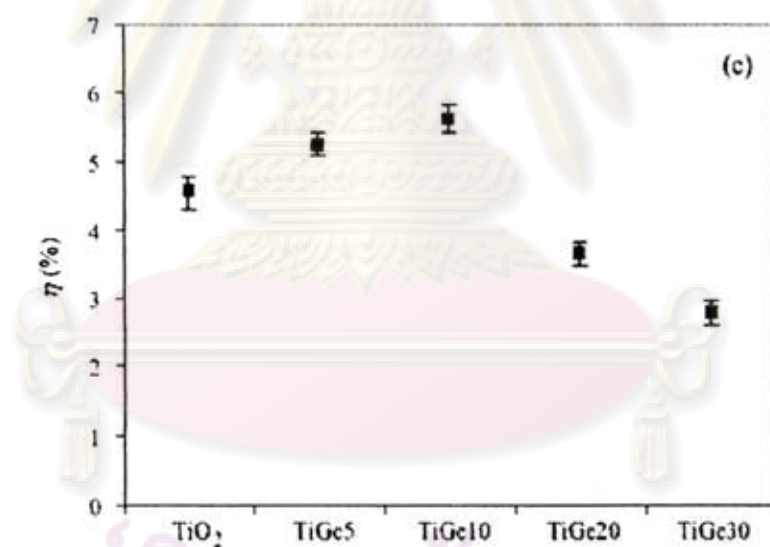


Figure 2.11 Relation between of overall efficiency of cell and oxide composition (Kitiyanan et al., 2006)

ศูนย์วิทยทรัพยากร
จุฬาลงกรณ์มหาวิทยาลัย

In general, one of the major limitations in semiconductor photocatalysis is the relatively low value of the overall efficiency, because of the high recombination rate of photo-induced electron-hole pairs at or near its surface. To improve the performance of photocatalytic activity has been achieved by several methods, such as using nanoparticle semiconductor crystallites instead of bulk materials and modifying semiconductor by doping with ions to other oxides. These methods can greatly improve the separation rate of photo-induced charge carriers in semiconductor photocatalysts so that the photocatalytic activity increases.

The photoluminescence (PL) technique has been widely used in photoactivity for study the electronic structure, optical and photochemical properties of semiconductor materials by which information such as surface oxygen vacancies, defects and the efficiency of charge carrier trapping.

It is well known that the PL signals of semiconductor materials result from the recombination of photo-induced charge carriers. In general, the lower the PL intensity with the lower the recombination rate of photo-induced electron-hole pairs, and higher the photocatalytic.

The some factors effect of PL process such as material size and dopant species. PL spectrum on TiO_2 at different sintering temperature (seen in Figure 2.12) show that when sintering temperature increased with PL spectrum decreased, which relate to the increased in particle sized (Liqiang et al., 2006).

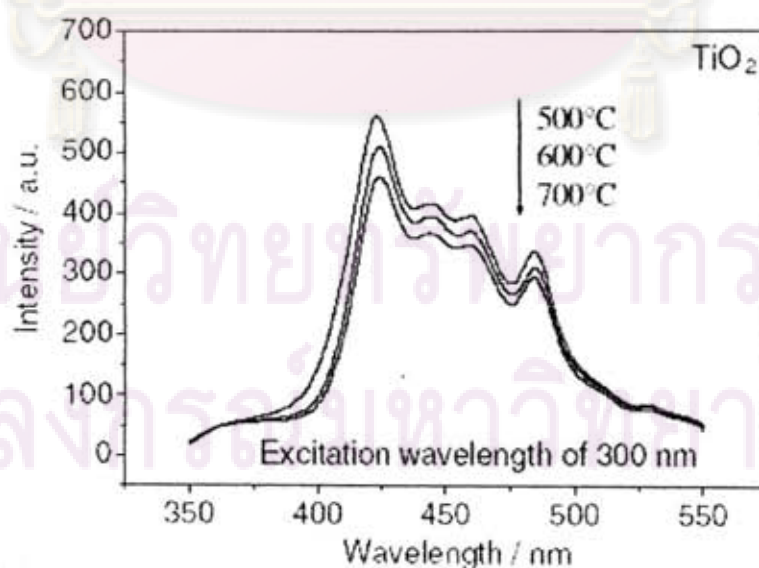


Figure 2.12 PL spectra of TiO_2 nanoparticles with the excitation wavelength at 300 nm (Liqiang et al., 2006)

The effects of dopant have three types, dopant (I) whose stable chemical state easily captures electron such as ceria (Ce). PL spectra of Ce-doped TiO₂ nanoparticles calcined at 600^oC (seen in Figure 2.13). It show that PL intensity decreases after an amount of Ce increased. Also, the dopant (II), Whose are the coupling material of two kinds of semiconductors such as WO₃ doped TiO₂ nanoparticles calcined at 500^oC (seen in Figure 2.14). It found that amount of W increases with PL intensity decreases. The basis of the relevant band positions of WO₃ and TiO₂, photo-induced electrons easily transfer from TiO₂ conduction band to WO₃ conduction band. Hence, photo-induced electrons and holes can be efficiently separated with PL signals go down (Liqiang et al., 2006).

The dopant (III), whose stable chemical state but it cannot capture electrons such as La³⁺, it can greatly influence PL spectra of nano-sized semiconductor materials due to the stronger the PL spectrum, the higher the content of surface oxygen vacancy and defect (seen in Figure 2.15). The PL intensity of La dope TiO₂ show that the highest intensity, indicating recombination of electron and hole has been promoted in La dope TiO₂.

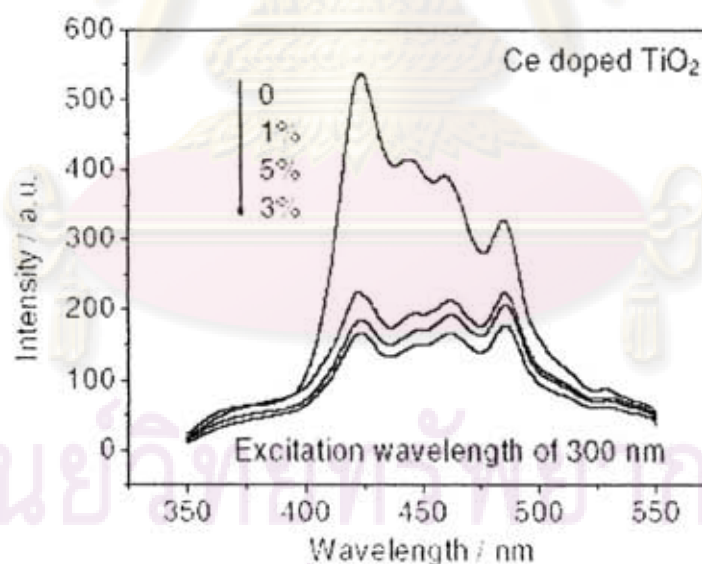


Figure 2.13 PL spectra of Ce doped TiO₂ at the excitation wavelength of 300 nm (Liqiang et al., 2006)

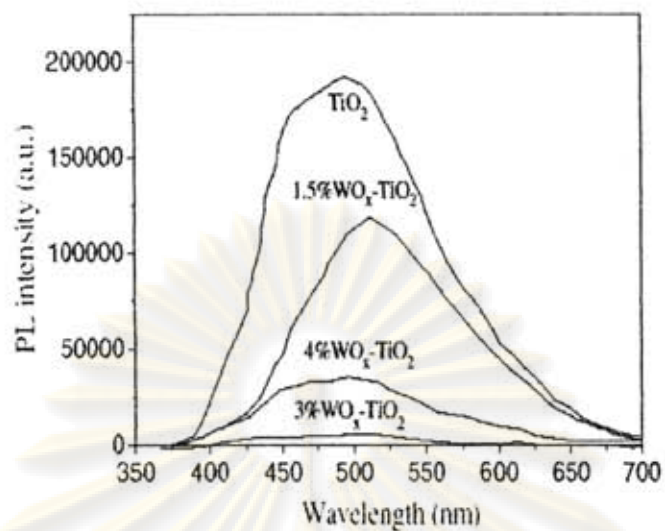


Figure 2.14 PL spectra of W-doped TiO_2 at the excitation wavelength of 325 nm
(Liqiang et al., 2006)

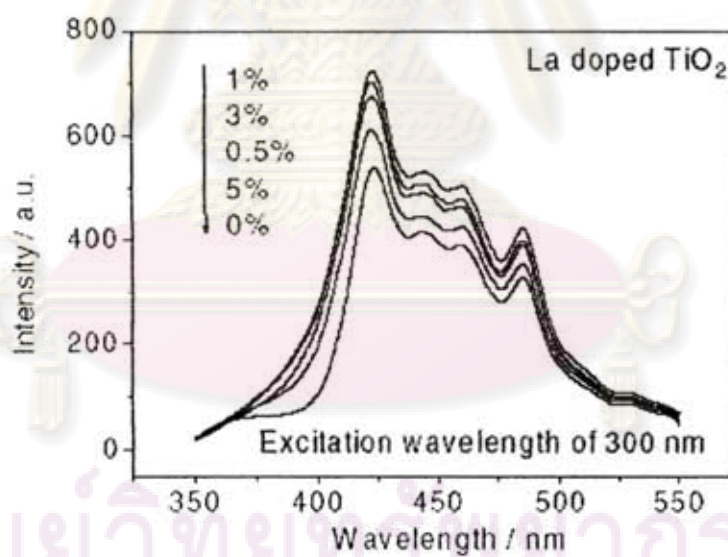


Figure 2.15 PL spectra of La doped TiO_2 at the excitation wavelength of 300 nm
(Liqiang et al., 2006)

CHAPTER III

EXPERIMENTAL

This chapter discussed various materials and methods employed in this research. The chapter was divided into three parts including preparation of TiO_2 film and metal oxide doped TiO_2 film, fabrication of dye sensitized solar cell and characterization techniques employed in this study.

3.1 Preparation of TiO_2 film and metal oxide doped TiO_2 film

The preparation of the TiO_2 film and metal oxide doped TiO_2 film consisted of two steps: the preparation of TiO_2 sol via sol gel and the application of TiO_2 sol onto electrode by ultrasonic spray coating.

3.1.1 Preparation of TiO_2 sol

TiO_2 sol was prepared via a sol-gel method. A solution consisted of 14.44 ml of 70% nitric acid and 2000 ml of distilled water. Titanium (IV) isopropoxide in the amount of 166.80 ml was added slowly into the solution while being stirred continuously at room temperature. The mixture solution was stirred for 3-4 days until clean sol was obtained. Next, the clean sol underwent dialysis in a cellulose membrane. The distilled water used for dialysis was changed daily until a pH 3.5 was obtained. And then, TiO_2 sol was kept in a refrigerator until needed.

3.1.2 Preparation of metal oxide doped TiO_2 sol

In this work added metal oxide doped TiO_2 film. The metal oxide chosen for this study were Fe_2O_3 , WO_3 and CeO_2 added to a TiO_2 sol at concentrations of 0.25%, 1% and 2% (w/w). This work assumed that one liter of TiO_2 contained 19 grams of TiO_2 particles.

3.1.2.1 Preparation of Fe₂O₃/TiO₂ sol

Preparation of Fe₂O₃ sol, this work mixed 83.8 g of Fe(NO₃)₃ in deionized water to make 250 ml solution (0.83 M of Fe(NO₃)₃ solution). Then the solution filtered through a glass micro-fiber filter (WhatmanGF/F). Add 83.2 ml of 5M NaOH rapidly to the iron solution, while being stirred continuously at room temperature for 40 minutes, after which the pH is approximately 1.5. Iron solution was kept in a refrigerator until needed.

To obtain 0.25%, 1%, and 2% (w/w) of Fe/Ti, this work mixed 0.07ml, 0.29 ml and 0.58 ml of iron solution with TiO₂ sol with the volumes of 87.5 ml, 86.84 ml, and 85.97 ml respectively. The solution was stirred until homogeneity was obtained. And then, the mixture solution underwent dialysis in a cellulose membrane until a pH 3.5 was obtained.

3.1.2.2 Preparation of WO₃/TiO₂ sol

Preparation of WO₃ sol by dissolving 1g of WCl₆ in 12.7 ml of ethanol while being stirred continuously at room temperature for 1 hour. Color of solution change from yellow to green and the final solution was blue.

To obtain 0.25%, 1%, and 2% (w/w) of W/Ti, this work mixed 0.07 ml, 0.27 ml and 0.57 ml of WO₃ solution with TiO₂ sol with the volumes of 87.5 ml, 86.84 ml, and 85.97 ml respectively. The solution was stirred until homogeneity was obtained. And then, the mixture solution underwent dialysis in a cellulose membrane until a pH 3.5 was obtained.

3.1.2.3 Preparation of CeO₂/TiO₂ sol

Preparation of CeO₂ sol by dissolving 0.5 g of Ce(NO₃)₃.6H₂O in 25 ml of distilled water while being stirred continuously until homogeneous solution, after its pH value was adjust to about 2 by using 5M of nitric acid solution.

To obtain 0.25%, 1%, and 2% (w/w) of Ce/Ti, this work mixed 1.21 ml, 4.83 ml and 9.67 ml of CeO₂ sol with TiO₂ sol with the volumes of 87.68 ml, 86.84 ml, and 85.96 ml respectively. The solution was stirred until homogeneity was obtained. And then, the mixture solution underwent dialysis in a cellulose membrane until a pH 3.5 was obtained.

3.2 Preparation of dye sensitized solar cell components and the fabrication procedure

The components of DSSC are mainly considered of transparent conducting glass, dye, electrolyte, counter electrode and anode electrode.

3.2.1 Transparent conducting glass

The conducting glass is transparent conducting oxide coated glass, which is the fluorine dope tin oxide (FTO) coated electrically conducting glass. The glass was purchased from Solaronix (Switzerland) under a commercial name TCO22-15. Identify the conducting side of fluorine dope tin oxide coated on glass by using a multimeter to measure resistance. The conducting side will have a sheet resistance is 15-20 ohm. The glass should not be touched by fingers, It was cleaned with ethanol and dried with a hair-dryer.

3.2.2 Dye

In this research, this work used Cis-di(thiocyanate)bis(2,2'-bipyridine-4,4'-dicarboxylate)ruthenium(II) or N3 (R535) dye from Solaronix was used. To prepare the dye solution, 20 mg of N3 dye was mixed with ethanol (Mecrk) 100 ml solution (0.3 mM of N3 dye solution). The solution was stirred until homogeneity was obtained.

3.2.3 Electrolyte

Electrolyte consisted of 0.5 M lithium iodine (LiI) (Fluka), 0.05 M iodide (I_2) (A.C.S reagent), and 0.5 M 4-tert-butylpyridine (TBP) in acetonitrile (A R Grade), 2.00 g of LiI, 0.38 g of I_2 , and 2.20 ml of TBP were mixed in 30 ml of acetonitrile. The solution was stirred until homogeneity was obtained.

3.2.4 Counter electrode

The counter electrode for the DSSC is platinum coated on conducting glass. To prepare a platinum counter electrode by ion sputtering, first this work cut a conducting glass to a rectangular piece that was $1.0 \times 1.5 \text{ cm}^2$. The glass clean with ethanol and dry with a hair-dryer. Then, tape was placed on one side of the glass as seen in Figure 3.1. Wipe off any fingerprints using a tissue wet with ethanol. Then, platinum target was sputtering on the conducting glass using ion sputtering (JEOL JFC-1100E) at 10 mA of ion current for four minutes. After sputtering, masking tape was removed.

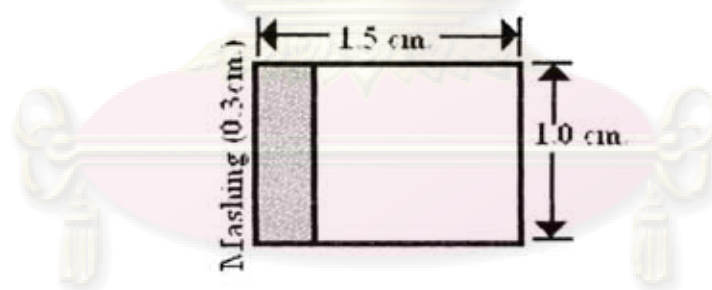


Figure 3.1 Show counter electrode before sputtering

ศูนย์วิจัยทรพยากร
จุฬาลงกรณ์มหาวิทยาลัย

3.2.5 Working electrode

Anode electrode consisted of TiO_2 film or metal oxide dope TiO_2 film on a conducting glass. To prepare the anode electrode, first this work cut a conducting glass into a rectangular piece that was $1.0 \times 1.5 \text{ cm}^2$. The glass clean with ethanol and dry with a hair-dryer. Then the glass was masked with aluminum foil to a circle have radius 0.5 cm as seen in Figure 3.2. The cut out was located closer to one side of the foil than the other.

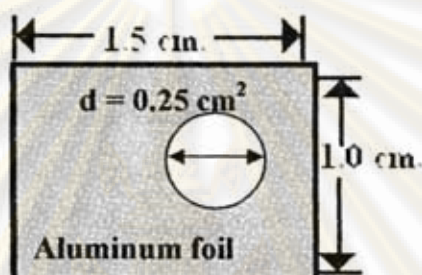


Figure 3.2 Show working electrode before spray coating

After masking, TiO_2 was coated on the conducting glass using ultrasonic spray coater. Stir well the TiO_2 sol before use, not shake unless bubbles could be formed. The spraying liquid such as TiO_2 sol was placed in a syringe pump, which fed the liquid at a rate 1 ml/min to an ultrasonic nozzle. The level speed of a moving stage was 4. The power of an ultrasonic nozzle, provided by a frequency generator until, was 3.5 watts.

This study effect of film thickness then this work varied number of coats of TiO_2 sol at 100, 150, 200, and 250 coats. The numbers of coats before each drying are five by a hair dryer. The thickness of film was measured using profilometer (Veeco Dektak 150).

The coat conducting glasses were calcined in air at a temperature ranging from $300 \text{ }^\circ\text{C}$ to $600 \text{ }^\circ\text{C}$ for two hours. After that electrodes were left to be cooled to $30 \text{ }^\circ\text{C}$. Before dye impregnation, this work heat electrode on hotplate at $70 \text{ }^\circ\text{C}$ for 10 minute, to avoid water absorption. Put slowly the anode electrode was immersed in a solution of 0.3 mM N3 dye for 10 hours in the dark then the anode electrode rinse with ethanol (the ethanol remove water from the porous TiO_2) and dry with hair-dryer.

3.2.6 Fabrication of dye sensitized solar cell assembly

Assembly the two electrodes (counter and anode electrode), First this work cut two strips of a sealing material that were 0.15 cm wide and 1.2 cm long. The strips were inserted as spacer between the platinum counter electrode and anode electrode. The platinum counter electrode was placed on top of the anode electrode so that the conducting side of the counter electrode was on top of the TiO_2 film. The cell was sealed by heating the sealing material with a hotplate at 60°C for 3 minute (see Figure 3.3).

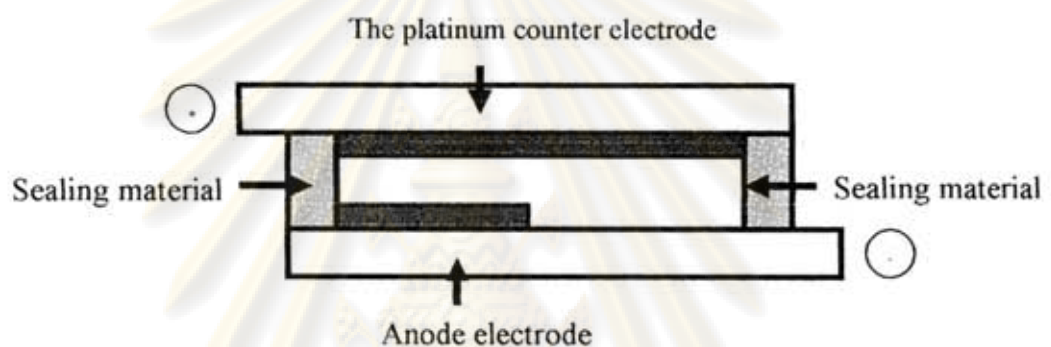


Figure 3.3 Cross-section of assembled dye solar cell showing sealing rim

For electrolyte filling, in cell having a sealing rim with two small holes, the filling is done by putting a droplet onto only one hole, and let it soak up (see Figure 3.4), then clean carefully the area around the filling holes with acetone. The cell is ready for testing.

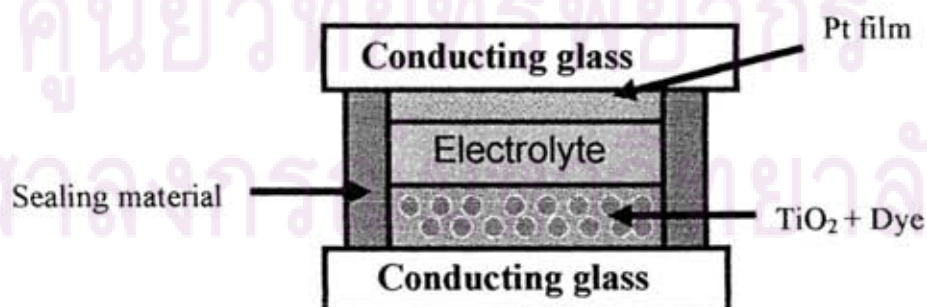


Figure 3.4 Fabrication of dye sensitized solar cell assembly for testing

3.3. Physical and Electrochemical Characterization

In this section discussed various techniques for physical and electrochemical properties of TiO₂, metal oxide dope TiO₂ and DSSC, various characterization techniques were employed.

3.3.1 X-ray diffractometry (XRD)

XRD was performed to determine crystal phase and crystallite size of TiO₂, CeO₂/TiO₂, Fe₂O₃/TiO₂ and WO₃/TiO₂. It was conducted using a SIEMENS D5000 X-ray diffractometer with Cu K_α radiation ($\lambda = 1.54439 \text{ \AA}$) with Ni filter. The spectra were scanned at a rate of $0.04^\circ \text{ min}^{-1}$ in the 2θ range of $20\text{-}80^\circ$.

3.3.2 Nitrogen physisorption

To determine the specific surface area of TiO₂, CeO₂/TiO₂, Fe₂O₃/TiO₂ and WO₃/TiO₂ were measured through nitrogen gas adsorption in a continuous flow method at liquid nitrogen temperature. A mixture of nitrogen and helium was employed as the carrier gas using Micromeritics ChemiSorb 2750 Pulse Chemisorption System instrument. The sample was thermally treated at 200°C for one hour before measurement.

3.3.3 UV-Visible Absorption Spectroscopy (UV-Vis)

The amount of dye adsorption was determined by a spectroscopic method by measuring the concentration of dye desorbed on the titania film into a mixed solution of 0.1M NaOH and ethanol (1:1 in volume fraction). The absorption spectra was measured by UV-Vis Absorption Spectroscopy (Perkin Elmer Lampda 650, λ between 300-800 nm and step size 1 nm).

3.3.4 Photoluminescence (PL)

To study the recombination of electrons–holes, photoluminescence measurement was carried out on a Fluorescence spectrophotometer (Perkin–Elmer LS-55) by using a Xenon lamp as the excitation source at room temperature and the excitation wavelength used in photoluminescence (PL) measurement was 300 nm.

3.3.5 Inductively Coupled Plasma-Atomic Emission Spectroscopy (ICP-AES)

The amount of metal deposited on the surface of titanium dioxide was measured with an Optima 2100 DV spectrometer. The sample was solution, this work dissolved 0.01 g of catalyst in 5 ml of 49% hydrofluoric acid (Merck) stirred until homogenous solution then the solution make to 100 ml with deionized water. The solution has concentration of 5 ppm (mg.l^{-1}) from the catalyst which was assumed to have metal content of 2wt%.

The standard solutions were prepared from 100 ppm standard of Fe solution, 1,000 ppm standard of Ce solution and 1,000 ppm standard of W solution (Perkin Elmer). Example preparation of the standard Fe solution was diluted to the concentration of 0.1, 0.5, 1, 2 and 3 ppm from 100 ppm of standard of Fe solution. This work 1.5 ml of the standard Fe solution make to 50 ml with deionized water (3 ppm of the standard Fe solution). For the reagent blank was 5 ml of hydrofluoric acid make to 100 ml with deionized water.

3.3.6 Scanning electron microscope (SEM)

The particle morphology was observed using a Hitachi S-3400 scanning electron microscope (SEM) operated at 15.0 keV.

จุฬาลงกรณ์มหาวิทยาลัย

3.3.7 Current-Voltage Tester (I-V Tester)

The electrochemical properties of dye sensitized solar cell were determined by I-V tester Current–voltage measurements were performed using white light source under air mass (AM) 1.5G conditions. To determine current density, open circuit voltage, cell resistance, and fill factor. This information was then converted to efficiency of the solar cell. An area of our solar cell was 0.196 cm^2 . The equipment used was MV Systems Inc., Xenon short ARC (Osram XBO 1000 W/HS).



ศูนย์วิจัยทรัพยากร
จุฬาลงกรณ์มหาวิทยาลัย

CHAPTER IV

RESULTS AND DISCUSSION

In this chapter, the experimental results and discussion were described and divided into three major parts, namely, influence of sintering temperature, influence of thickness of electrode layer and influence of adding of Fe_2O_3 , WO_3 and CeO_2 to TiO_2 electrode layer on the performance of dye sensitized solar cell.

4.1 Effect of sintering temperature on TiO_2 electrode layer

TiO_2 sol was prepared via sol-gel method. It has been used as a working electrode in DSSC. In general, sintering temperature affect on photocurrent-voltage characteristic because of the change of crystalline size and surface area of titania (Ngamsinlapasathian et al., 2005). In this study, the sintering temperature was varied to be 300 °C, 400 °C, 500 °C and 600 °C for 2 h.

The results from XRD analysis of all the TiO_2 powders calcined at different temperature for 2 h were shown in Figure 4.1.

Figure 4.1 showed that the XRD patterns at 2θ values of 25.32°, 37.88°, 48.16° and 62.80° corresponded to the anatase phase, whereas the XRD peak at 2θ values of 27.44 °, 41.28 ° and 54.36° belonged to rutile phase and XRD peak at 2θ values of 30.88° belonged to brookite phase (Porkodi and Arokiamary, 2007).

The average crystallite size of anatase was estimated from the half-height width of (101) diffraction peaks of anatase at 2θ values of 25.32° using the Scherrer's equation. Next, this work determined specific surface area of TiO_2 powders from nitrogen adsorption technique. The results are crystallite size, weight fraction of anatase, rutie and brookite phase and surface area presented in Table 4.1, this table showed that the crystallite sizes and weight fraction of rutile of TiO_2 increases while weight fraction of anatase and surface area of TiO_2 decreases with increasing sintering temperature.

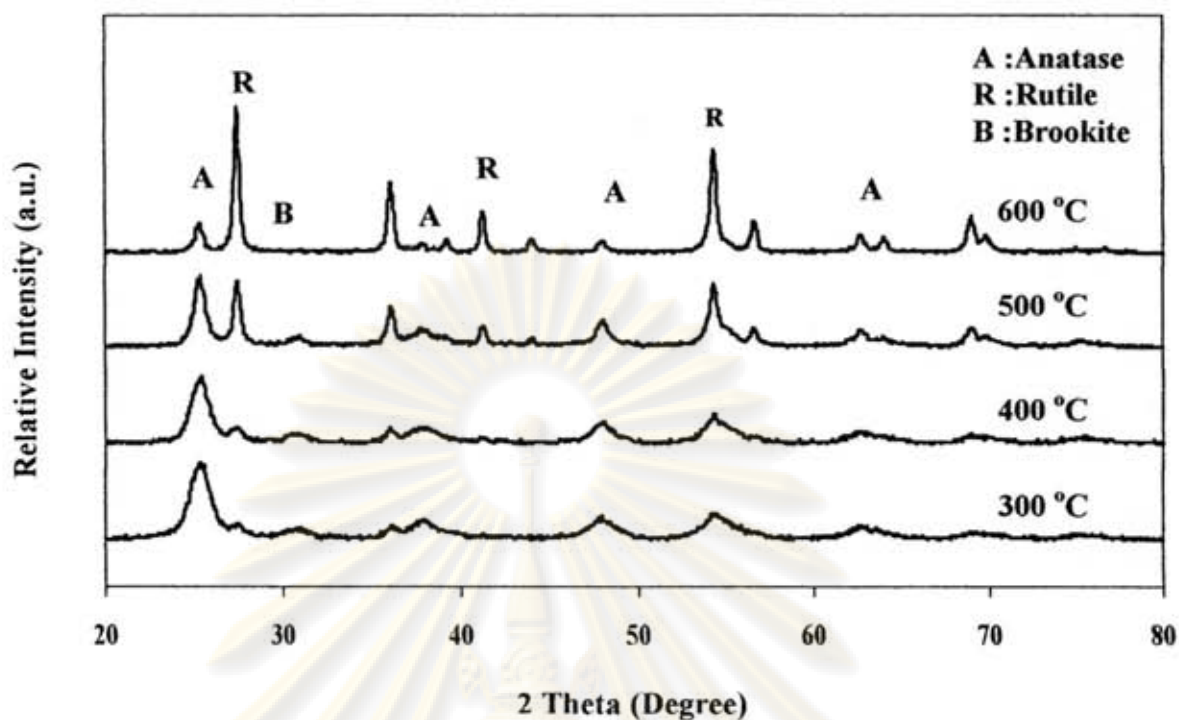


Figure 4.1 XRD patterns of TiO₂ powders sintered at different temperature

Table 4.1 Crystal size, surface area and weight fraction of anatase, rutile and brookite phase of TiO₂ powders sintered at various temperatures for 2 h

Sintering temperature of TiO ₂ (°C)	Crystallite size (nm)	Surface area (m ² /g)	W _A	W _R	W _B
300	6.2	124.1	0.60	0.14	0.26
400	7.3	88.1	0.58	0.16	0.26
500	11.6	63.1	0.40	0.41	0.19
600	18.4	25.1	0.15	0.81	0.04

W_A : weight fraction of anatase phase

W_R : weight fraction of rutile phase

W_B : weight fraction of brookite phase

จุฬาลงกรณ์มหาวิทยาลัย

Surface morphologies of TiO_2 obtained by SEM for different sintering temperatures were shown in Figure 4.2. The SEM image of TiO_2 calcined at 600°C showed that the formation of the large TiO_2 particle cause many small nanoparticle are sintered together with increasing sintering temperature and correlated with the phase transformation of TiO_2 nanoparticle from anatase to rutile (Lee et al., 2007).

The increasing of particle size can be attributed of crystallization of the surface amorphous structure and the connections of those small nanoparticles at higher sintering temperature are important for help electron transport of TiO_2 film electrode (Zhao et al., 2008).

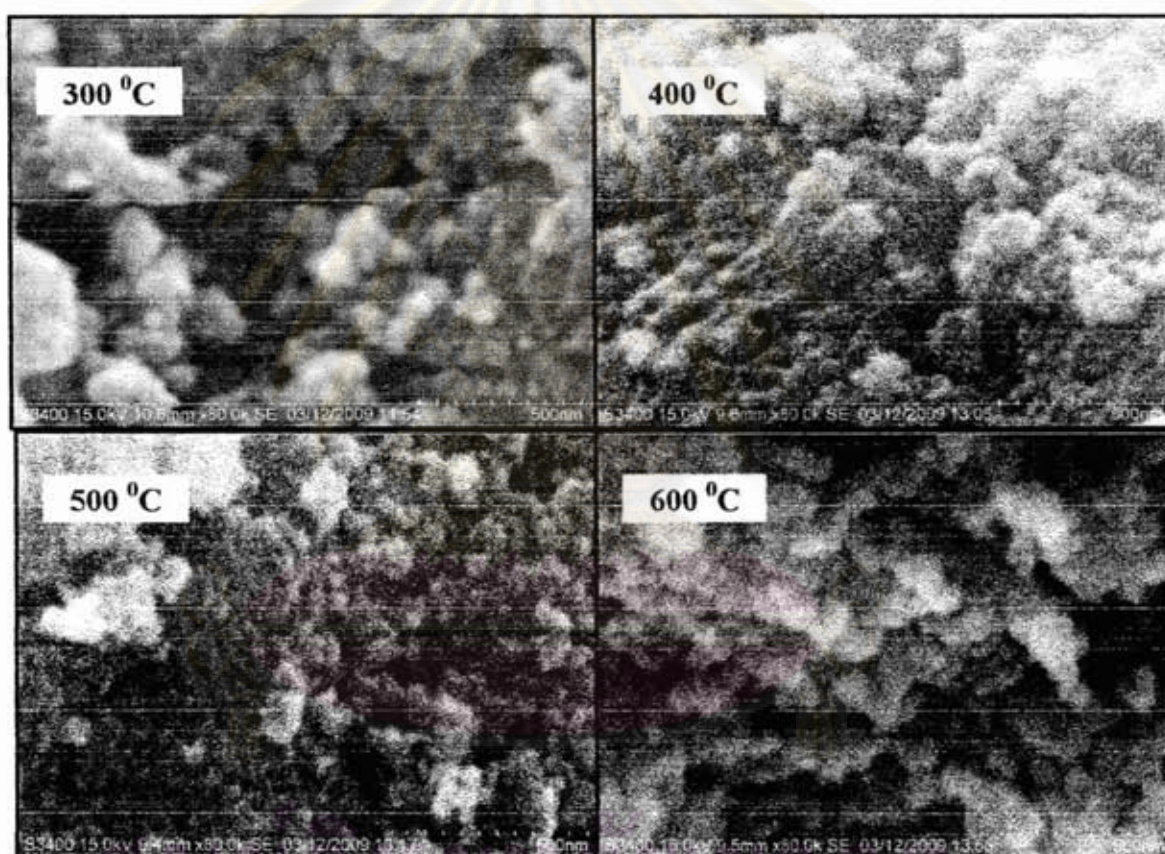


Figure 4.2 SEM images of TiO_2 powders calcined at different temperatures

For this study, the electrode consisted of 100 coats of TiO_2 have film thickness was approximately $1.74 \mu\text{m}$ at various sintering temperature indicated that increasing sintering temperature with decreases amount of dye absorption on TiO_2 surface were shown in Figure 4.3.

The dye absorption on TiO_2 surface was maximal up to 400°C can be understood from FTIR spectra. From Figures 4.4 showed the FTIR spectra of TiO_2 calcined at $300, 400, 500$ and 600°C respectively. The FTIR spectra possessed peaks at $970, 1653, 3400,$ and 3700 cm^{-1} . The peak at 970 cm^{-1} corresponding to Ti-O-Ti bonds and the peak at 3700 cm^{-1} corresponding to Ti-OH on surface of TiO_2 . The water and the OH groups around 1653 and 3400 cm^{-1} were present respectively (Zhang et al., 2002).

After calcination at temperature higher than 300°C , the vibration bands of water and surface hydroxyl groups became much weaker. Therefore, surface hydroxyl group and water in TiO_2 were removed during calcinations. The lower adsorption of water on surface of TiO_2 with sintering temperature increases may be associated with an increases of available surface sites for dye adsorption. Hence the TiO_2 calcined at 400°C can be adsorbed of dye was higher than the TiO_2 calcined at 300°C (N-Park et al., 2000).

The PL spectra is useful in explain the efficiency of charge carrier trapping, immigration and transfer and the electron-hole pairs in semiconductor particle. The PL spectra of TiO_2 sintered at different temperature were shown in Figure 4.4. It can be seen that the PL intensity of TiO_2 decreased with increased sintering temperature which indicated that the recombination of excited electron and hole decreases when the particle size increases due to increased sintering temperature (Liqiang et al., 2006 and Zhao et al., 2008).

ศูนย์วิจัยทรัพยากร
จุฬาลงกรณ์มหาวิทยาลัย

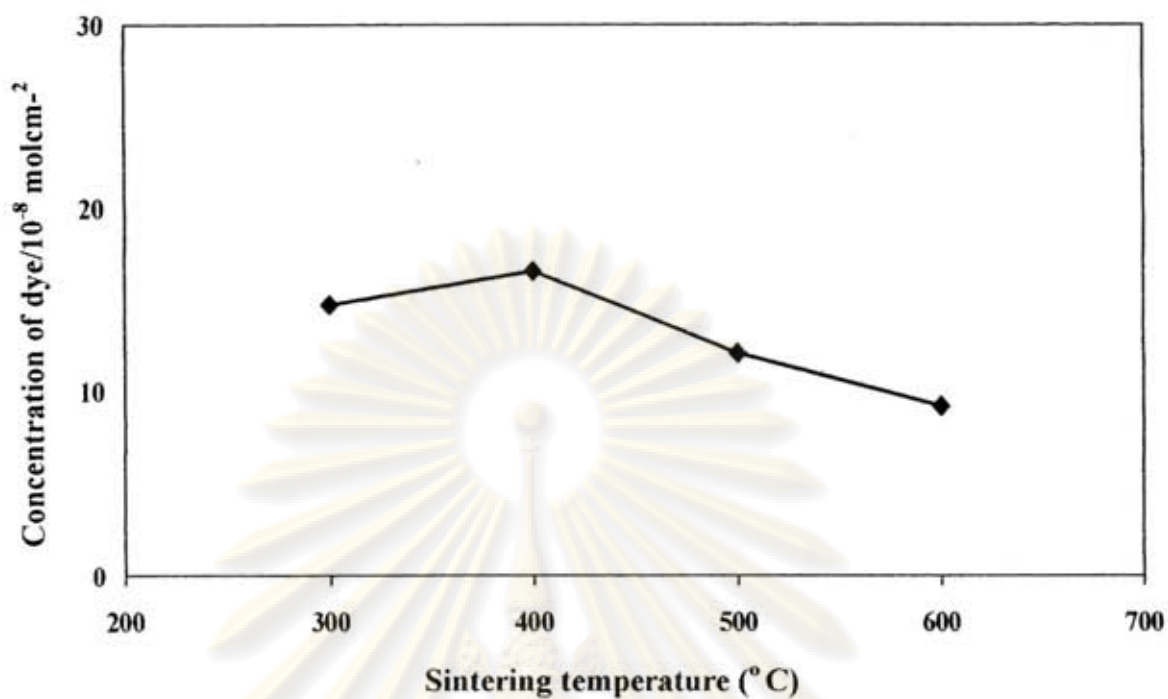


Figure 4.3 Relationship between concentrations of dye and sintering temperatures with 100 coats of TiO_2 electrodes layer

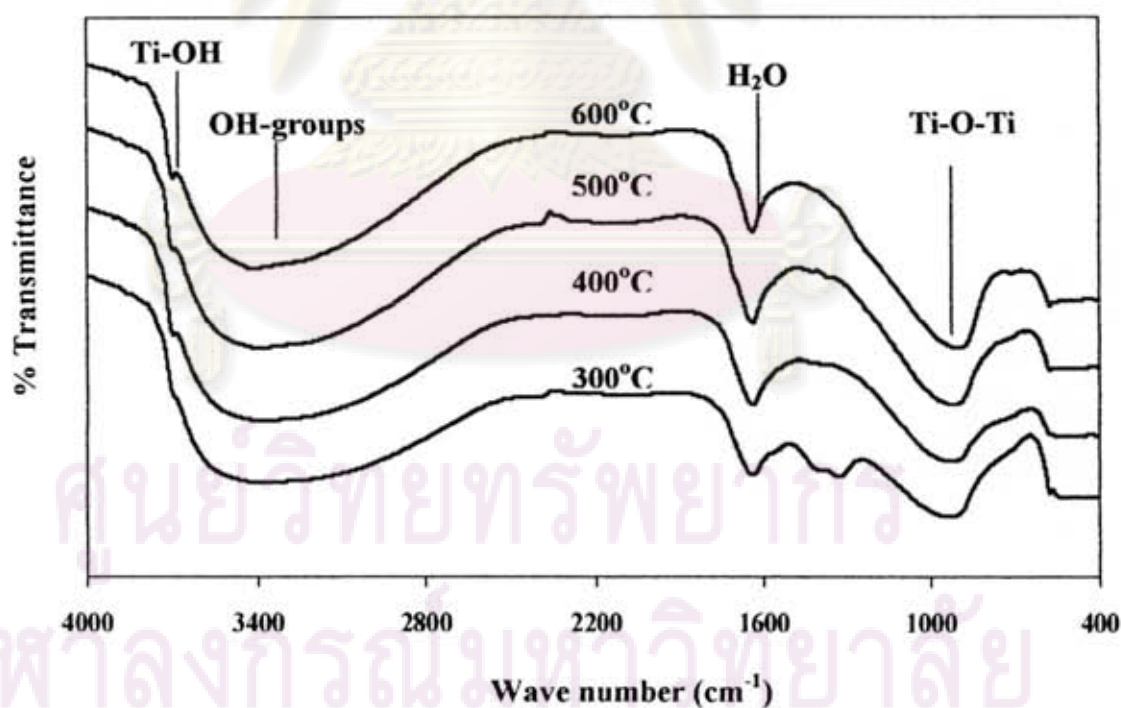


Figure 4.4 FTIR spectra of TiO_2 calcined at different temperatures

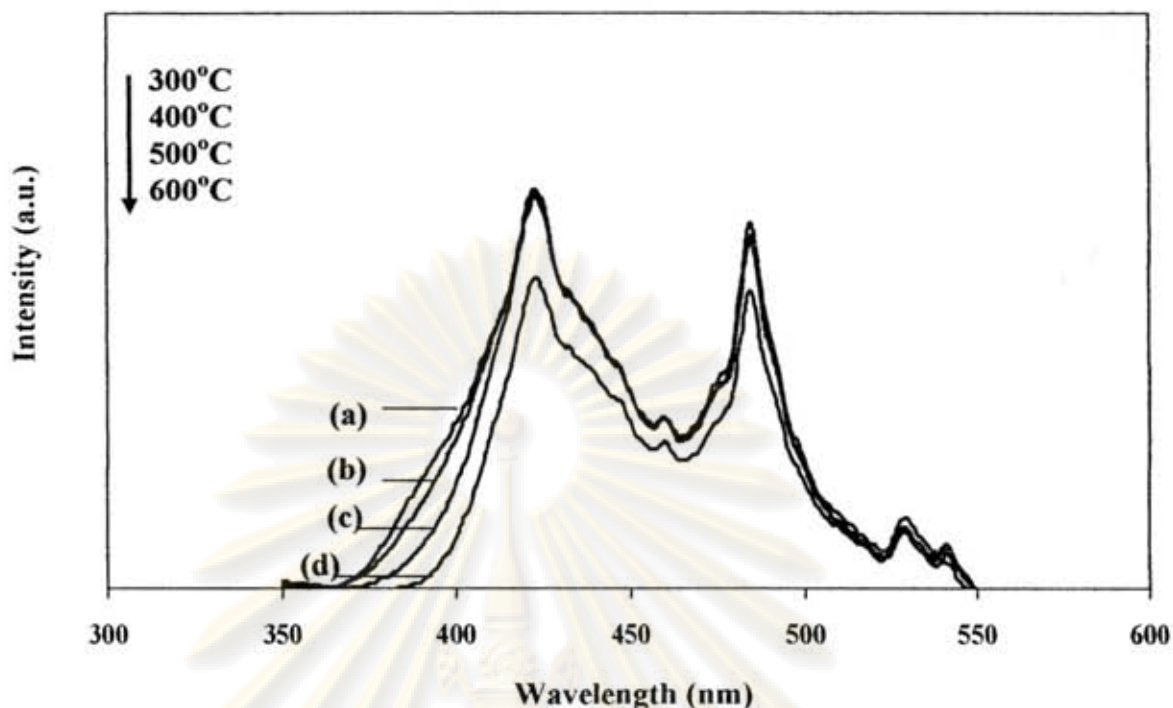


Figure 4.5 PL spectra of TiO₂ calcined at different temperature of (a) 300°C, (b) 400°C, (c) 500°C and (d) 600°C

The resulting of electrochemical properties in Table 4.2 of the thickness of TiO₂ was about 1.74 μm at various sintering temperature for 2 h indicated that sintering temperature influence on performance of DSSC, this table were shown photoelectrochemical characteristic such as short-circuit current (I_{SC}); open-circuit voltage (V_{OC}), fill factor (FF) and η (efficiency) of DSSC.

The photocurrent characteristic (I_{SC}) increases maximal up to 400°C and it decreases with increases in sintering temperature. Although surface area of the cell calcined at 400°C less than the cell calcined at 300°C, in contrast the amount of dye adsorption of electrode sintered at 400°C higher than the electrode sintered at 300°C. In general, the amount of adsorbed dye increases related with number of inject electron in metal electrode leading to an increase of I_{SC} (Kitiyanan et al., 2006). Hence, the electrodes calcined at 400°C improve the connection between particles which help electron transport of TiO₂ film electrode (Zhao et al., 2008).

The efficiency of the cell sintered at 500°C and 600°C decreases were shown in Figure 4.5) because of the increasing of rutile phase were shown in Table 4.1 leading to large particle size, less of surface area which due to absorption of dyes not enough. Beside, the electron transport of rutile film is slower than in anatase film, it cause current density decreases with the performance of dye sensitized decreases (Park et al., 2000).

Table 4.2 Electrochemical properties of DSSC with TiO₂ electrode calcined at various temperatures, the thickness of TiO₂ was about 1.74 μm

Sintering temperature of TiO ₂ (°C)	V _{oc} (Volt)	I _{sc} (mA/cm ²)	Fill Factor	Efficiency (%)
300	0.69	1.79	0.60	0.73±0.04
400	0.75	1.93	0.65	0.95±0.11
500	0.72	1.67	0.63	0.85±0.15
600	0.78	1.21	0.60	0.62±0.10

In this study three samples were used, and the efficiency of cell given is the average value follow by the standard derivation.

ศูนย์วิทยทรัพยากร
จุฬาลงกรณ์มหาวิทยาลัย

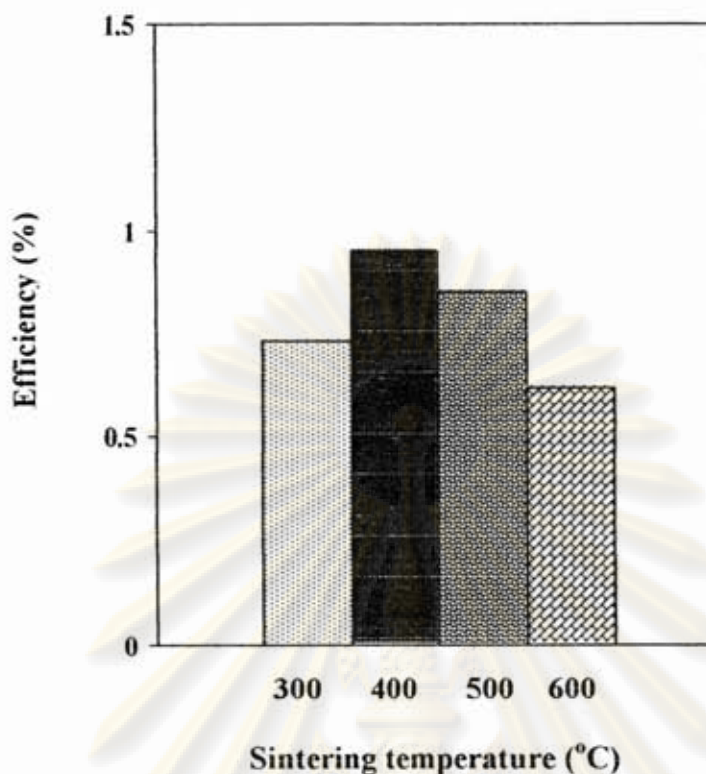


Figure 4.6 Efficiency of DSSC of TiO₂ calcined at different temperature

4.2 Effect of thickness of TiO₂ film

In this part, this work varied the thickness of TiO₂ electrode layer by varying number of coats of TiO₂ sprayed on the substrate. The numbers of coats of TiO₂ for this study were 100, 150, 200 and 250 coats and the electrode sintered at 400°C. The film thickness was measured using step profilometer.

From Figure 4.6 found that concentration of dye on TiO₂ surface increases with increasing thickness of film due to increasing of the film thickness leading to increasing the surface area of TiO₂ electrode (Kang et al., 2004).

The result of electrochemical properties of dye sensitized solar cells of TiO₂ were shown in Table 4.3, this table were shown that the increasing of film thickness with increases of I_{SC} which related to the increase injection current from excited dyes to the conduction band of TiO₂.

The efficiency of the cell increases linearly with the thickness increases were shown in Figure 4.7. The overall view of concentration of adsorbed dyes and the efficiency of cell at various sintering temperature and various film thickness were shown in Figure 4.8 and 4.9 indicated that increasing of film thickness related with number of coat, increasing of concentration of dye and increasing of the efficiency of TiO_2 electrode for every sintering temperature.

The TiO_2 electrode sintered at 400°C , the thickness was about $5.05\ \mu\text{m}$ gave the best solar energy conversion efficiency of 2.74 %.

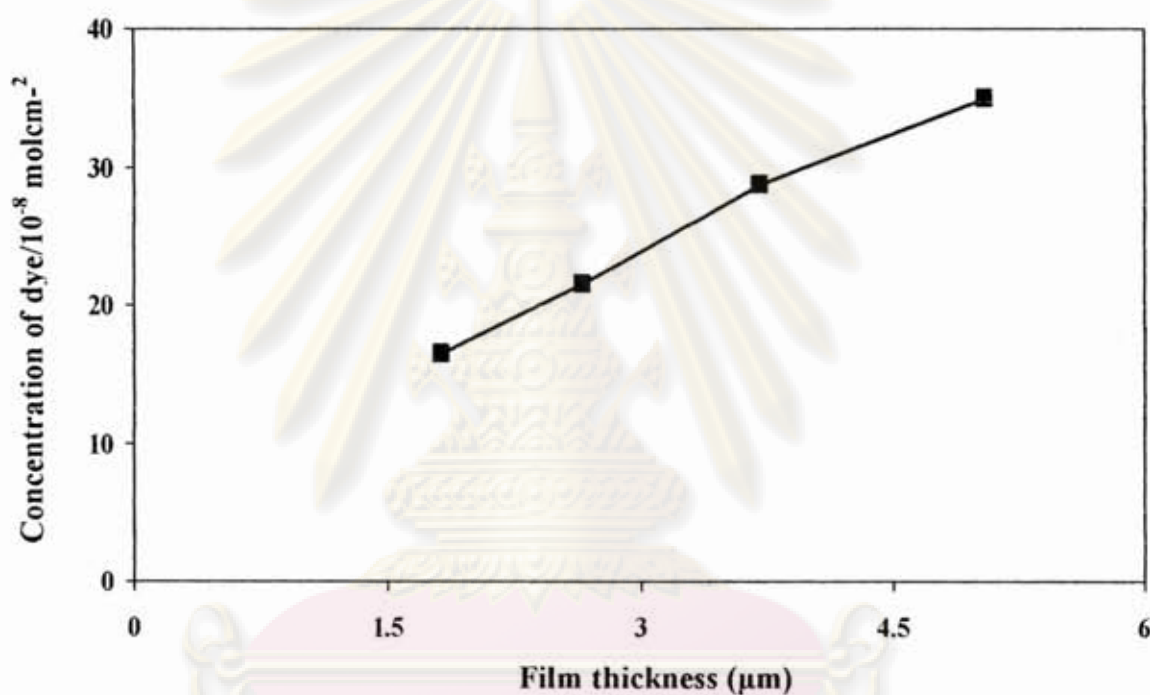


Figure 4.7 Relationship between concentrations of dye with various thicknesses of TiO_2 film

ศูนย์วิทยทรัพยากร
จุฬาลงกรณ์มหาวิทยาลัย

Table 4.3 Electrochemical properties of dye sensitized solar cells of TiO₂ electrode calcined at 400°C with various thicknesses

Film thickness (μm)	V _{OC} (Volt)	I _{SC} (mA/cm ²)	Fill Factor	Efficiency (%)
1.74	0.75	1.93	0.65	0.95±0.11
2.66	0.76	2.67	0.70	1.42±0.02
3.71	0.74	3.53	0.73	1.91±0.08
5.05	0.73	4.62	0.81	2.74±0.21

In this study three samples were used, and the efficiency of cell given is the average value follow by the standard derivation.

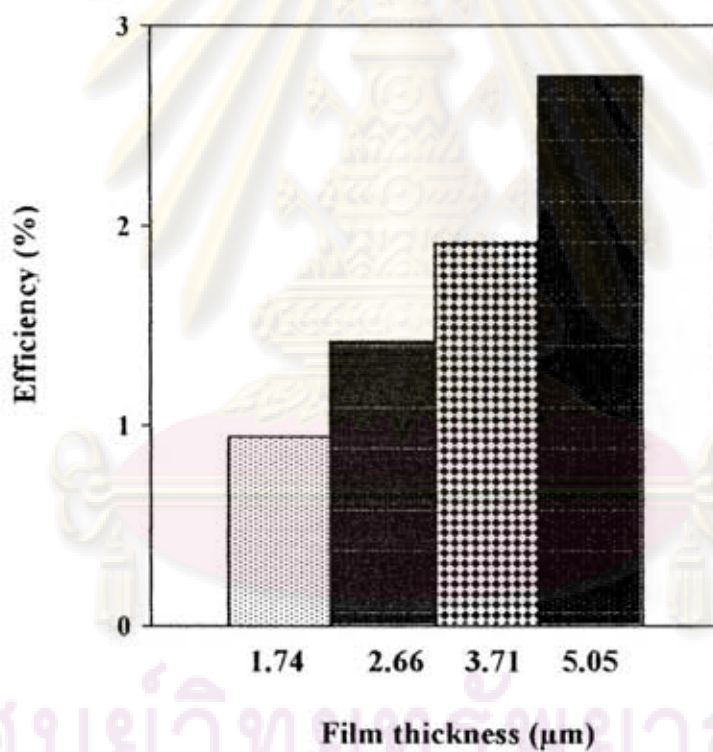


Figure 4.8 Efficiency of DSSC as a film thickness of TiO₂ for the electrode

ศูนย์วิทยุโทรพยากร
จุฬาลงกรณ์มหาวิทยาลัย

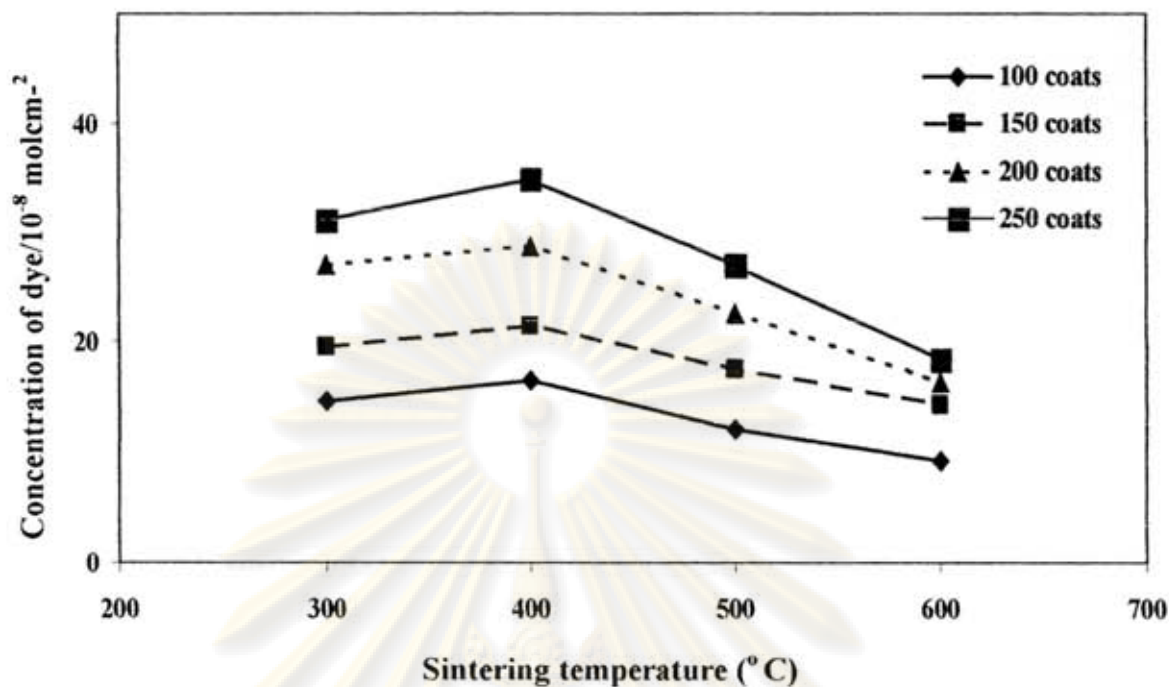


Figure 4.9 Relationship between concentrations of dye, sintering temperature ($^{\circ}\text{C}$) and number of coat of TiO_2 electrode

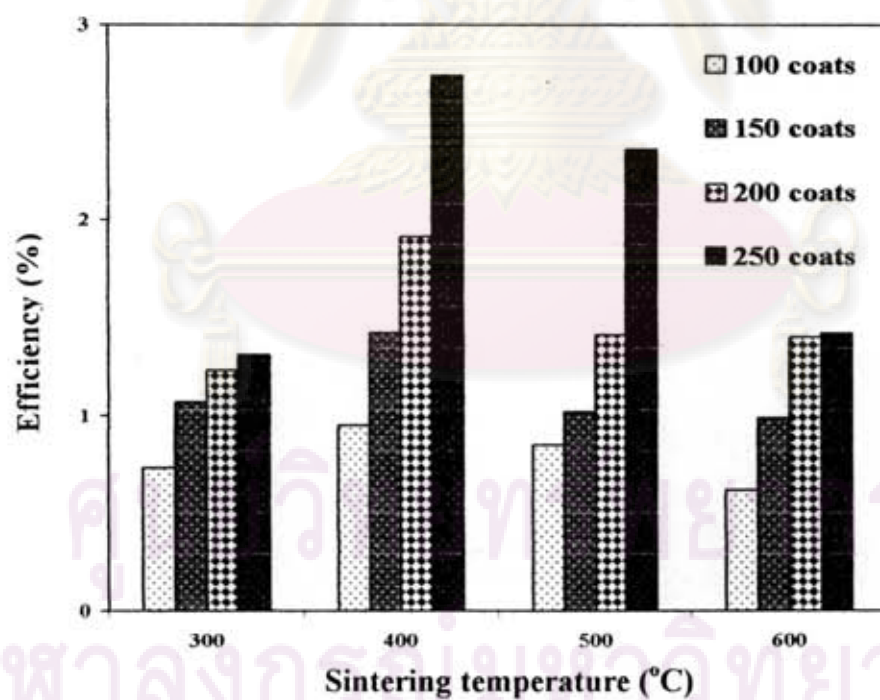


Figure 4.10 Efficiency of DSSC as a film thickness and sintering temperature of TiO_2 electrode

4.3 Effect of modification of TiO₂ electrode layer

4.3.1 Modification of TiO₂ electrode layer by Fe₂O₃

TiO₂ electrode layer was modified by addition of Fe₂O₃ to TiO₂ electrode at the percentage of Fe/Ti was 0.25 wt%, 1.0 wt% and 2.0 wt%, the electrode calcined at 400°C which sintering temperature gave highest the efficiency of DSSC, while still study influence of film thickness on performance of DSSC.

The XRD pattern of TiO₂ and Fe₂O₃/TiO₂ were display in Figure 4.10. The major phase of all samples was anatase. The results from XRD showed that weight fraction of anatase phase increases when the doping of Fe₂O₃ increases (see in Table 4.4). It imply that the doping of Fe₂O₃ inhibited the phase transformation of TiO₂ from anatase to rutile and the added ferric oxide role was based on the crystal growth inhibitor, which leading to small grain size correlated with high surface area due to the increasing of concentrations of dye when film thickness and percentage of Fe/Ti increases were shown in Figure 4.11.

The amount of Fe on Ti catalyst was determined using inductively coupled plasma atomic emission spectroscopy (ICP-AES). From ICP analysis the ratio of Fe/Ti atomic ratio of Fe₂O₃-TiO₂ mixed oxide calcined at 400°C for 2 h showed in Table 4.4. From result of ICP analysis found that the contents of Fe less than the nominal value may because the preparation of mixed oxide sol.

ศูนย์วิทยทรัพยากร
จุฬาลงกรณ์มหาวิทยาลัย

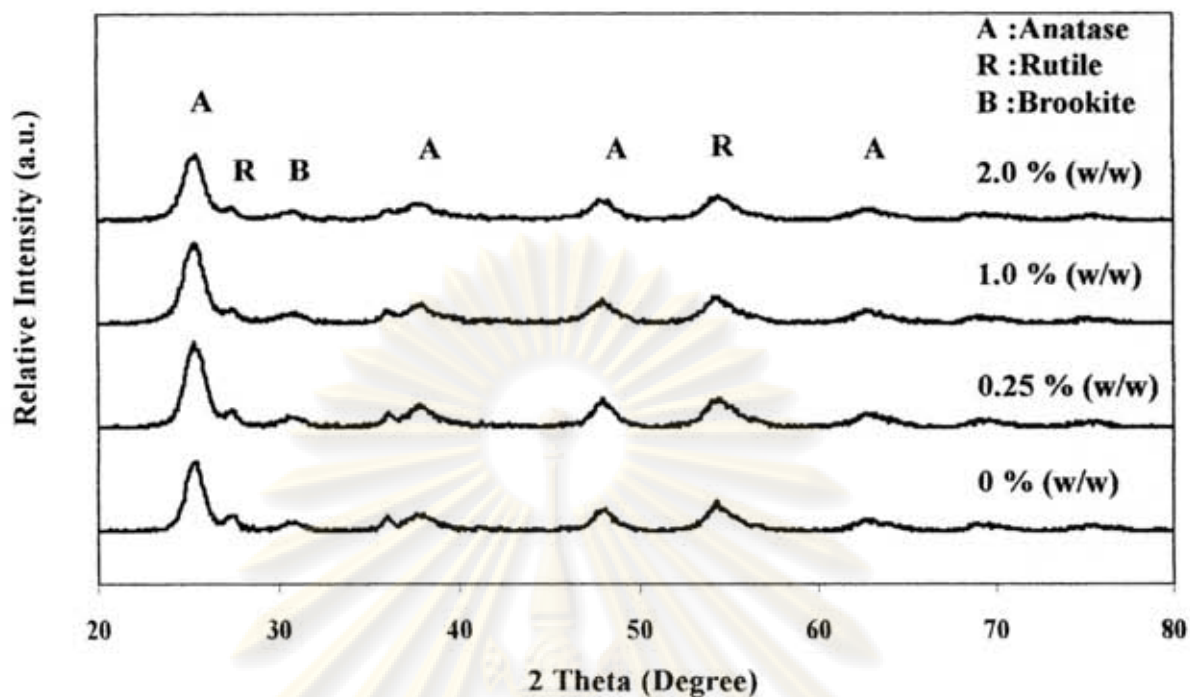


Figure 4.11 XRD patterns of Fe₂O₃/TiO₂ powders at various percentage of Fe/Ti.

Table 4.4 Crystal size, surface area and weight fraction of anatase, rutile and brookite phase of Fe₂O₃/TiO₂ powders sintered at 400°C for 2 h

Fe/Ti (wt%)	Crystallite size (nm)	Surface area (m ² /g)	Amount of Fe from ICP (wt%)	W _A	W _R	W _B
0	7.3	88.1	-	0.58	0.16	0.26
0.25	6.5	99.5	0.24	0.62	0.15	0.23
1	6.1	106.7	0.78	0.60	0.14	0.26
2	6.0	110.2	1.86	0.60	0.14	0.26

W_A : weight fraction of anatase phase

W_R : weight fraction of rutile phase

W_B : weight fraction of brookite phase

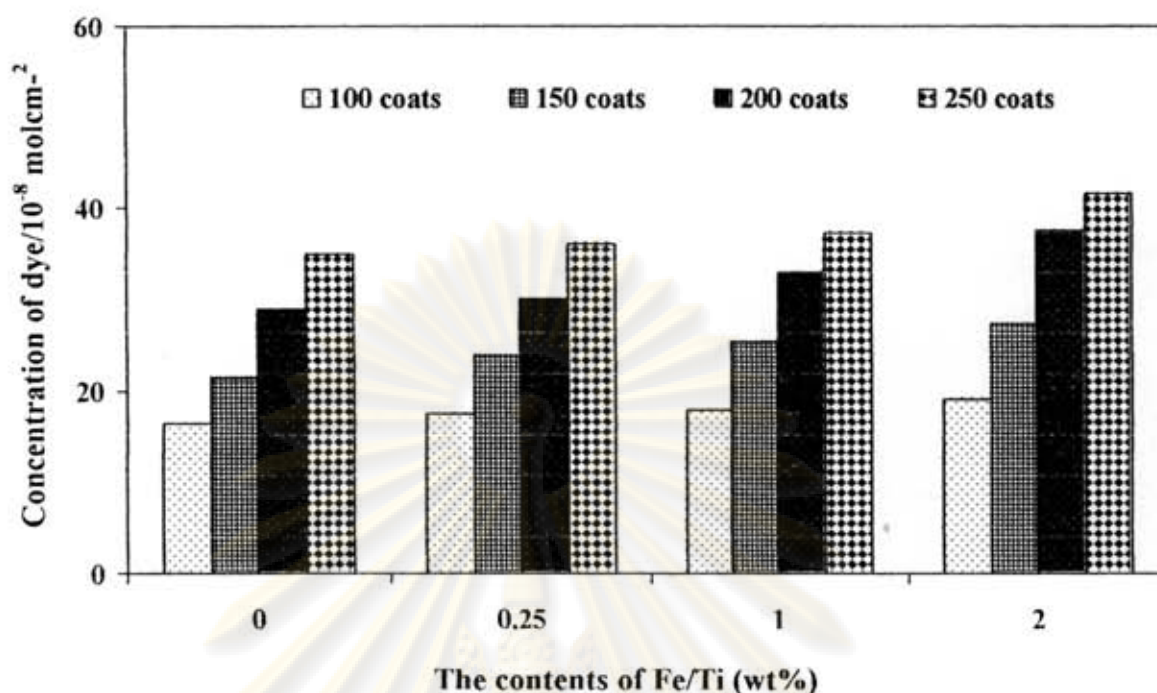


Figure 4.12 Relationship between concentrations of dye with various contents of Fe/Ti at different of number of coat of electrode

The result of PL intensity of 2.0 wt% Fe/Ti showed the highest rate combination of electron and hole (were shown in Figure 4.12). Increasing of the content of Fe with increased the PL intensity indicated that rate of recombination higher than pure TiO₂. It may be explained as that Fe act as recombination center for the photogenerated charge carriers (Wu et al., 2008), which match the result of electrochemical properties of Fe₂O₃/TiO₂ electrode calcined at 400°C with number of coats was 100, it found that amount of Fe increases with decreasing of I_{SC} and V_{OC} (were shown in Table 4.5). On the contrary, the I_{SC} increased with increasing of film thickness were shown in Table 4.6. Hence, the film thickness increase corresponding with high surface area, high amount of dye absorbed due to increasing of I_{SC}.

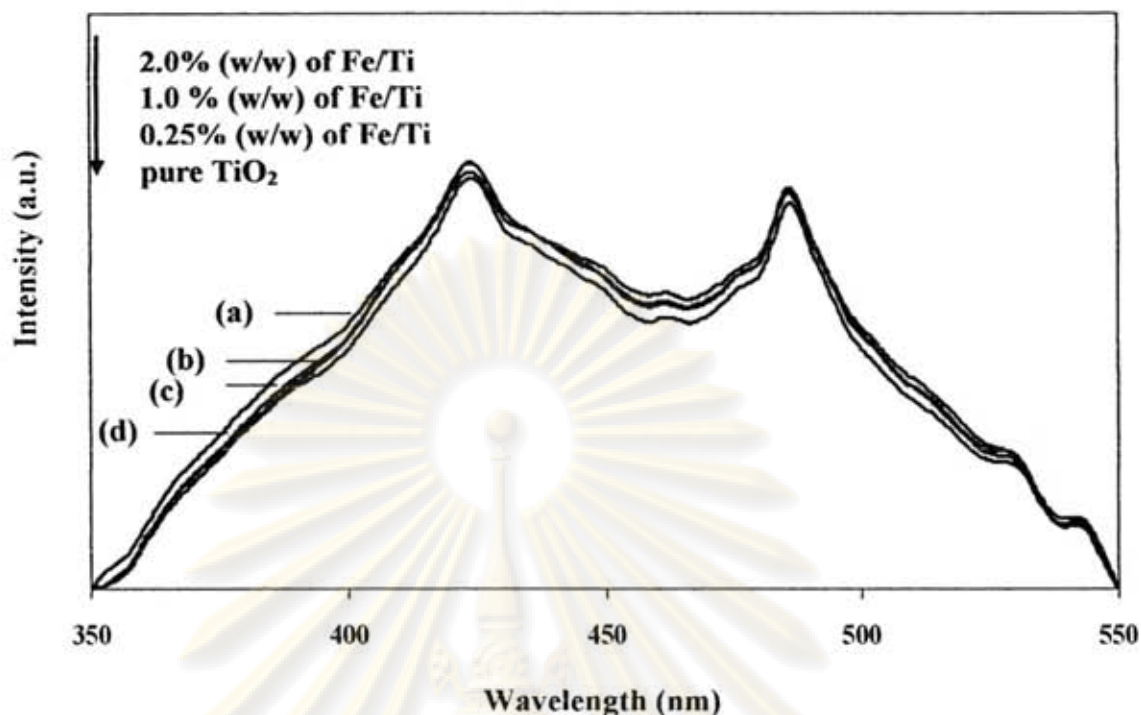


Figure 4.13 PL spectra of $\text{Fe}_2\text{O}_3/\text{TiO}_2$ at various contents of (a) pure TiO_2 , (b) 0.25% (w/w) of Fe/Ti, (c) 1% (w/w) of Fe/Ti and (d) 2% (w/w) of Fe/Ti

Table 4.5 Electrochemical properties of dye sensitized solar cells of $\text{Fe}_2\text{O}_3/\text{TiO}_2$ electrode calcined at 400°C with 100 coats

% Fe/Ti (w/w)	V_{oc} (Volt)	I_{sc} (mA/cm^2)	Fill Factor	Efficiency (%)
0	0.75	1.93	0.65	0.95 ± 0.11
0.25	0.49	0.49	0.60	0.14 ± 0.04
1	0.45	0.15	0.73	0.05 ± 0.01
2	0.43	0.1	0.54	0.02 ± 0.01

In this study three samples were used, and the efficiency of cell given is the average value follow by the standard derivation.

จุฬาลงกรณ์มหาวิทยาลัย

Table 4.6 Electrochemical properties of dye sensitized solar cells of 0.25wt% $\text{Fe}_2\text{O}_3/\text{TiO}_2$ electrode calcined at 400°C at various numbers of coats

Number of coat	V_{oc} (Volt)	I_{sc} (mA/cm^2)	Fill Factor	Efficiency (%)
100	0.49	0.49	0.60	0.14 ± 0.04
150	0.50	0.51	0.54	0.18 ± 0.03
200	0.48	0.64	0.64	0.20 ± 0.09
250	0.49	0.86	0.61	0.26 ± 0.03

In this study three samples were used, and the efficiency of cell given is the average value follow by the standard derivation.

Figure 4.13 showed the overall view of the efficiencies of dye sensitized solar cells of $\text{Fe}_2\text{O}_3/\text{TiO}_2$ electrode calcined at 400°C at various number of coat and the contents of Fe indicated that 2wt% of $\text{Fe}_2\text{O}_3/\text{TiO}_2$ electrode with number of coats were 100 gave less efficiency of cell. And, it possibly demonstrates that the rate of recombination of ferric is higher than titania which due to photocurrent density and open circuit decrease.

ศูนย์วิจัยทรัพยากร
จุฬาลงกรณ์มหาวิทยาลัย

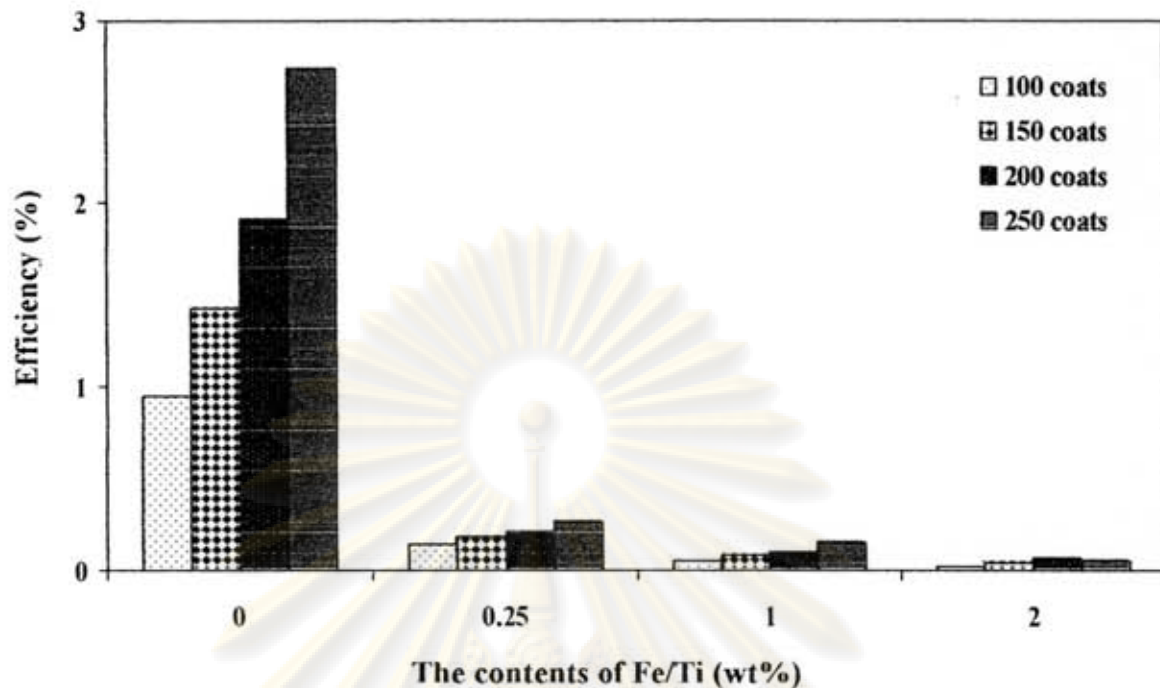


Figure 4.14 Efficiencies of dye sensitized solar cells of Fe₂O₃/TiO₂ electrode calcined at 400°C at various number of coat and the contents of Fe/Ti

4.3.2 Modification of TiO₂ electrode layer by adding WO₃

TiO₂ electrode layer was modified by addition of WO₃ to TiO₂ electrode at the percentage of W/Ti was 0.25 wt%, 1.0 wt% and 2.0 wt%, the electrode calcined at 400°C.

The XRD patterns of TiO₂ and WO₃/TiO₂ were display in Figure 4.17. It showed that the addition of tungsten into titania inhibited the phase transformation of TiO₂ from anatase to rutile.

Table 4.7 reported the various contents of W on Ti catalyst from ICP analysis, the crystallite size and surface area which the WO₃/TiO₂ had much higher surface areas than pure TiO₂. The higher surface areas can improve the ability of absorbed dyes were shown in Figure 4.11.

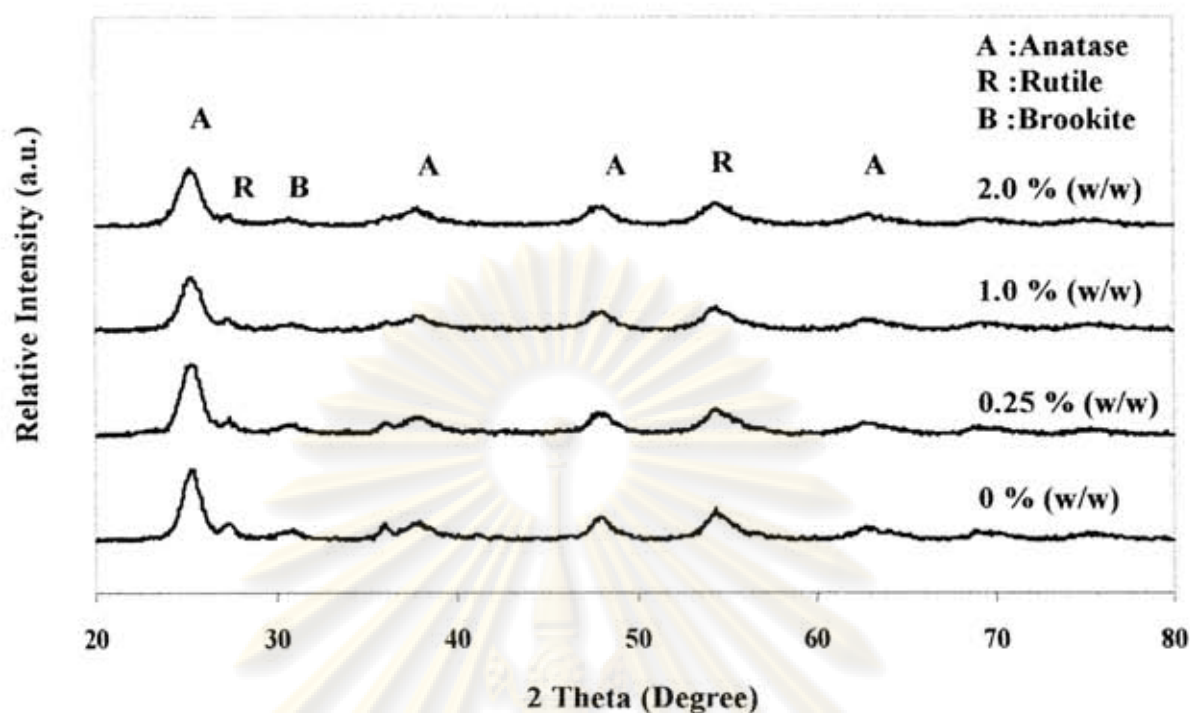


Figure 4.15 XRD patterns of WO_3/TiO_2 powders at various contents of W/Ti

Table 4.7 Crystal size, surface area and weight fraction of anatase, rutile and brookite phase of WO_3/TiO_2 powders sintered at 400°C for 2 h

W/Ti (wt%)	Crystallite size (nm)	Surface area (m^2/g)	Amount of W from ICP (wt%)	W_A	W_R	W_B
0	7.3	88.1	-	0.58	0.16	0.26
0.25	6.3	100.5	0.18	0.61	0.14	0.25
1	6.1	105.4	0.75	0.60	0.14	0.26
2	6.0	110.2	1.69	0.60	0.14	0.26

W_A : weight fraction of anatase phase

W_R : weight fraction of rutile phase

W_B : weight fraction of brookite phase

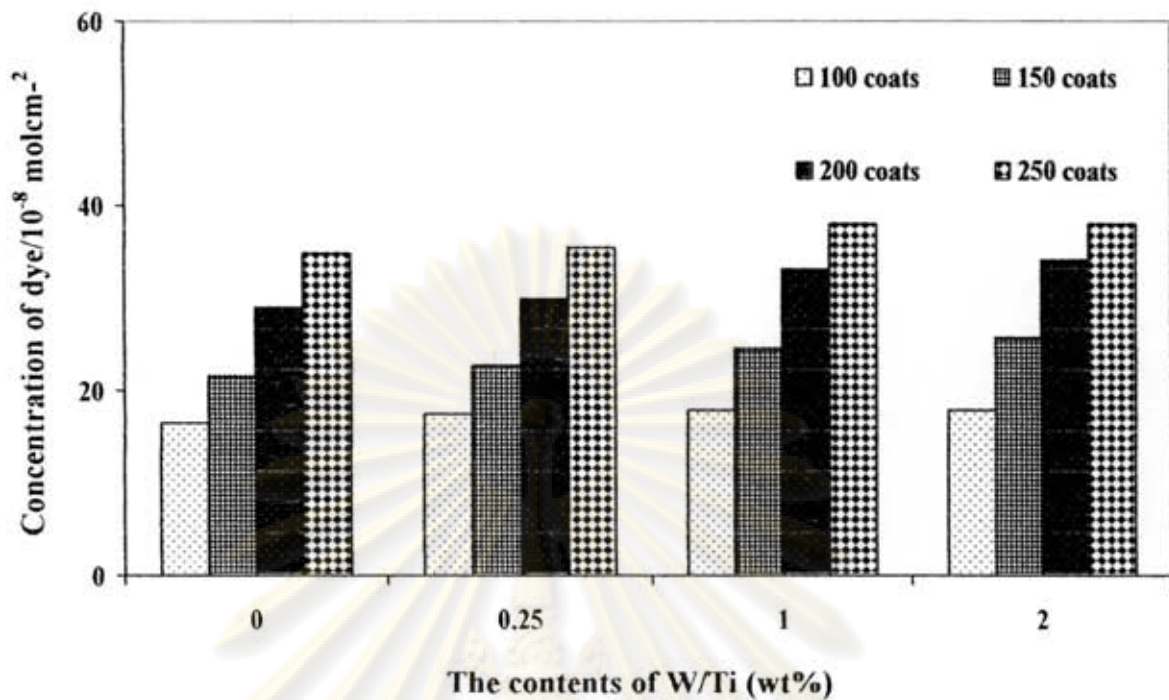


Figure 4.16 Relationship between concentrations of dye with various contents of W/Ti at different of number of coat of electrode

The PL emission spectra of all samples are shown in Fig. 4.12 found that PL spectrum of the pure TiO_2 is much higher than that in the spectra of addition tungsten samples. The PL intensity increased when the content of tungsten oxides increased and the content of tungsten at 2 wt% black slight decrease from 1 wt% of W/Ti. Thus imply that the addition of tungsten to improve the separation rate of photo-induced charge carriers in semiconductor. Hence, it can be photogeneration of electrons and holes were efficiently separated (Li et al., 2001, Liqiang et al., 2006 and Higashimoto et al., 2006).

ศูนย์วิทยทรัพยากร
จุฬาลงกรณ์มหาวิทยาลัย

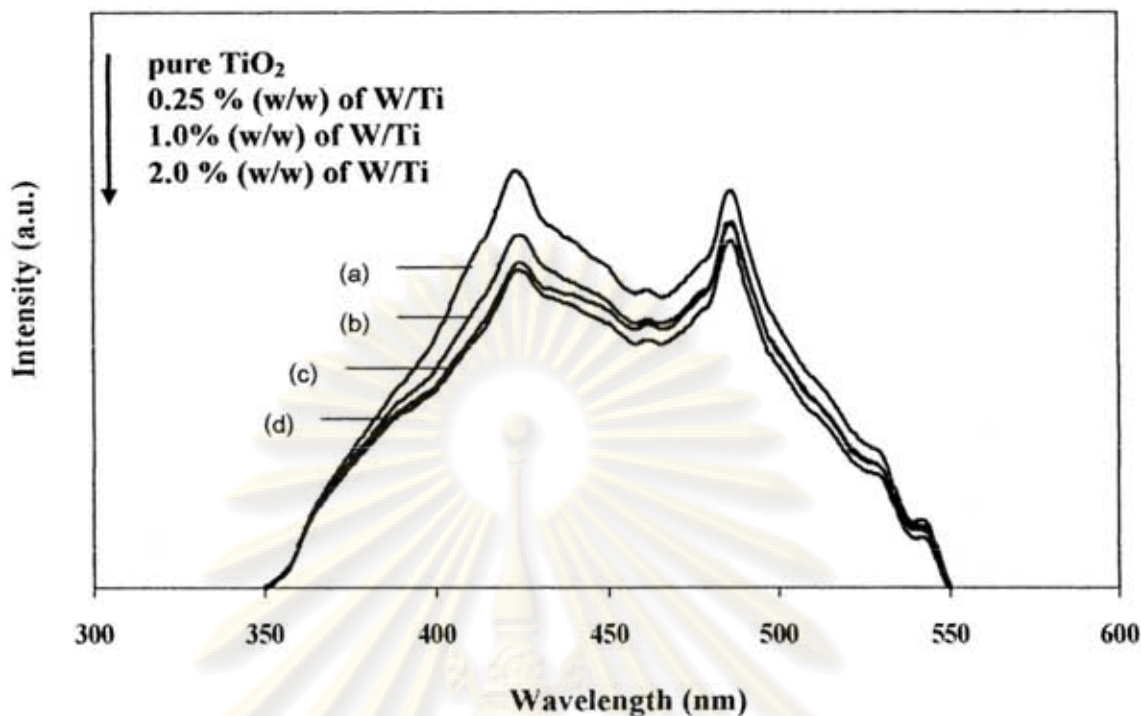


Figure 4.17 PL spectra of WO_3/TiO_2 at various contents of (a) pure TiO_2 , (b) 0.25% (w/w) of W/Ti, (c) 1% (w/w) of W/Ti and (d) 2% (w/w) of W/Ti

The results of the efficiency of cell can be explained in two case, first cases when number of coats when number of TiO_2 coats less than 150, it found that the overall efficiency of cell increases with the contents of tungsten increases, which maximal up 1wt% of W/Ti and it decreased with increasing of the amount of W due to optimum of efficiency. And last cases, when number of coats exceeded 150 indicated that the overall efficiency of cell decrease with the contents of tungsten increase which were shown in Figure 4.17. It can be understood from I_{SC} and V_{OC} value.

ศูนย์วิทยทรัพยากร
จุฬาลงกรณ์มหาวิทยาลัย

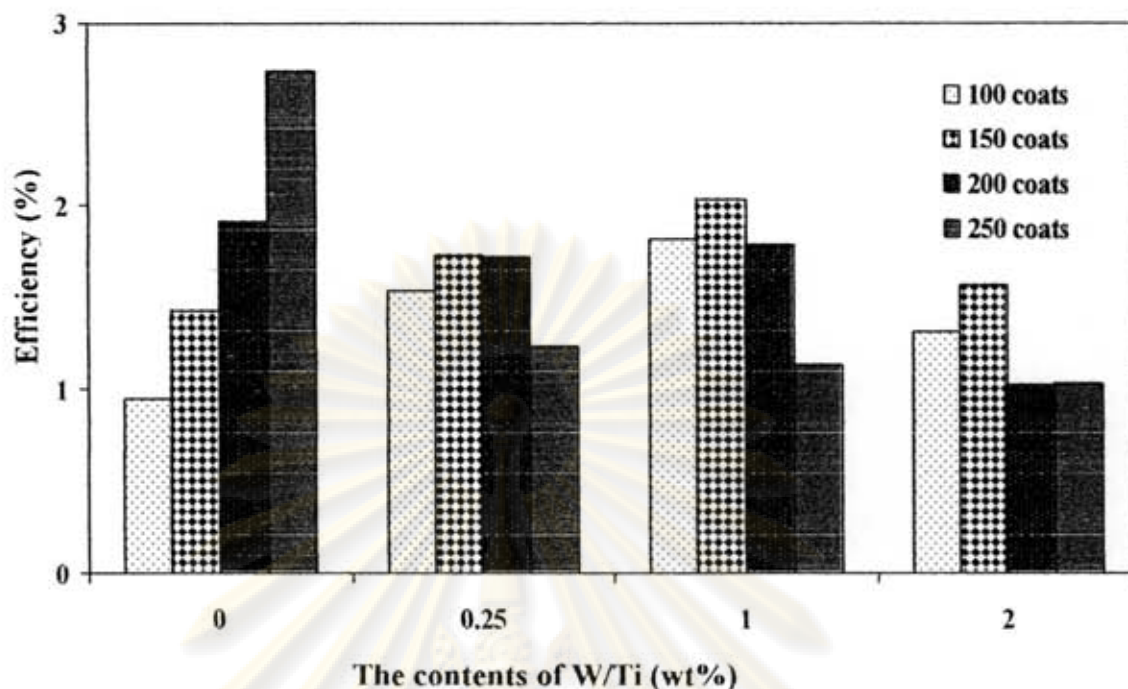


Figure 4.18 Efficiencies of dye sensitized solar cells of WO_3/TiO_2 electrode calcined at 400°C at various number of coat and the contents of W/Ti

First cases, the results of photovoltaic properties (V_{OC} and I_{SC}) were shown in Figure 4.18 and 4.19 indicated that the addition of tungsten increases with increasing of I_{SC} while the V_{OC} slight decreased, this result imply that the surface area was mainly responsible for the increases of the efficiency of cell.

In contrast, in the second cases were shown both of V_{OC} and I_{SC} decreased when the content of tungsten increase indicated that the surface area was not mainly responsible but it is probably due to the fact that, the charge recombination between electron injected from the excited dye to TiO_2 conduction band with hole and electron with I^{3-} ions in the electrolyte will become more serious in thicker film, which is detrimental to electron collection on the black contact and photocurrent generation (Kitiyanan et al., 2006).

จุฬาลงกรณ์มหาวิทยาลัย

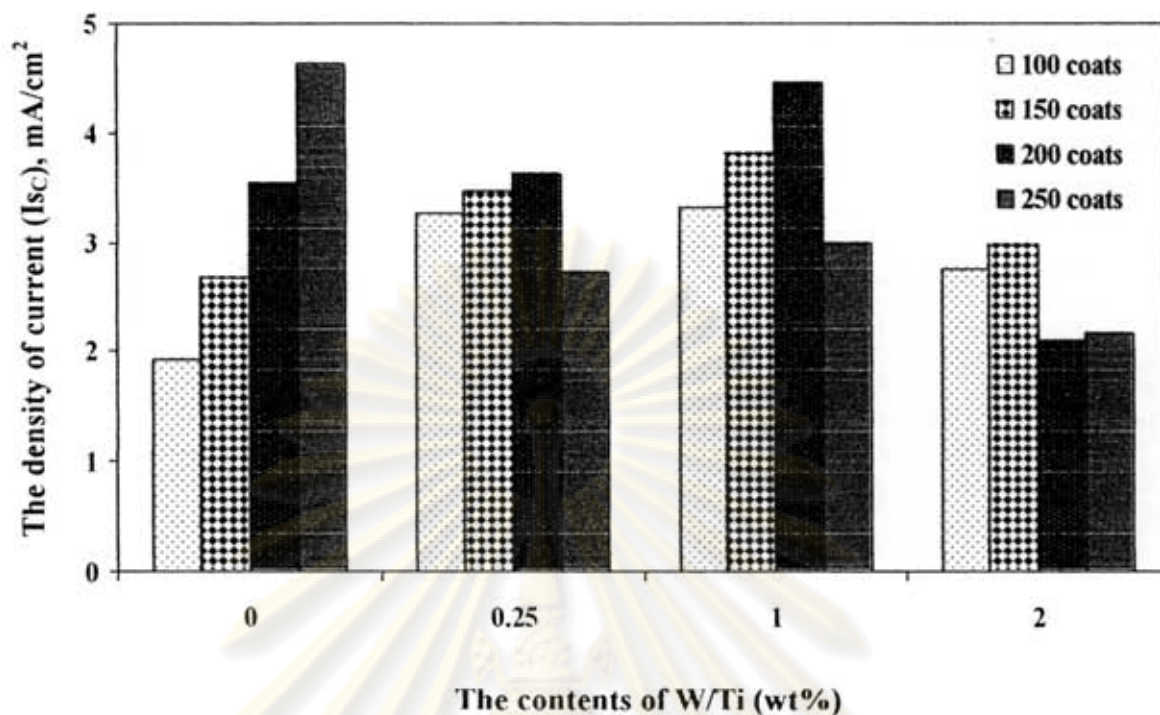


Figure 4.19 The density of current (I_{sc}) of cell of WO_3/TiO_2 electrode calcined at $400^\circ C$ at various number of coat and the contents of W/Ti

ศูนย์วิทยทรัพยากร
จุฬาลงกรณ์มหาวิทยาลัย

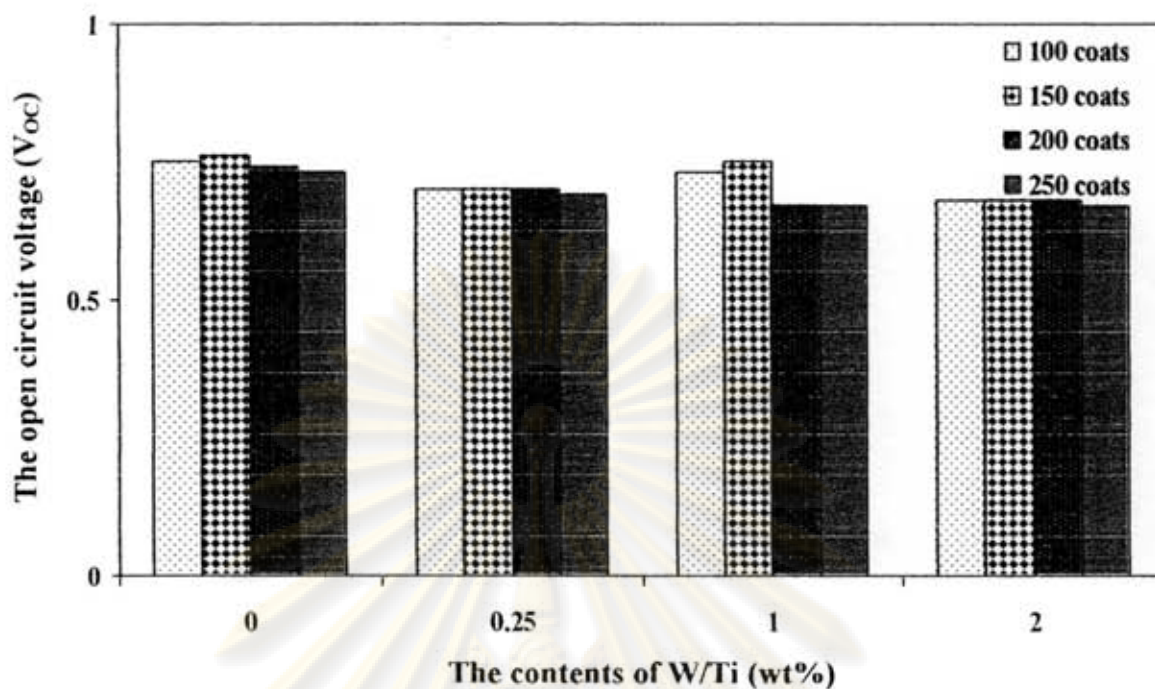


Figure 4.20 The open circuit voltage of WO_3/TiO_2 electrode calcined at 400°C at various number of coat and the contents of W/Ti

4.3.3 Modification of TiO_2 electrode layer by adding CeO_2

TiO_2 electrode layer was modified by addition of CeO_2 to TiO_2 electrode at the percentage of Ce/Ti was 0.25%, 1.0% and 2.0% (w/w), the electrode calcined at 400°C .

The XRD patterns of TiO_2 and $\text{CeO}_2/\text{TiO}_2$ were shown in Figure 4.20, indicated that the additions of ceria inhibited the phase transformation of TiO_2 from anatase to rutile up to 1 wt% of Ce/Ti which it was decrease with the content of ceria increase.

Table 4.8 reported the various contents of Ce on Ti catalyst from ICP analysis and this table showed that the crystallite size and surface area which The $\text{CeO}_2/\text{TiO}_2$ had much higher surface areas than pure TiO_2 . The higher surface areas related with increasing of the amount dye absorbed on TiO_2 surface were shown in Figure 4.21.

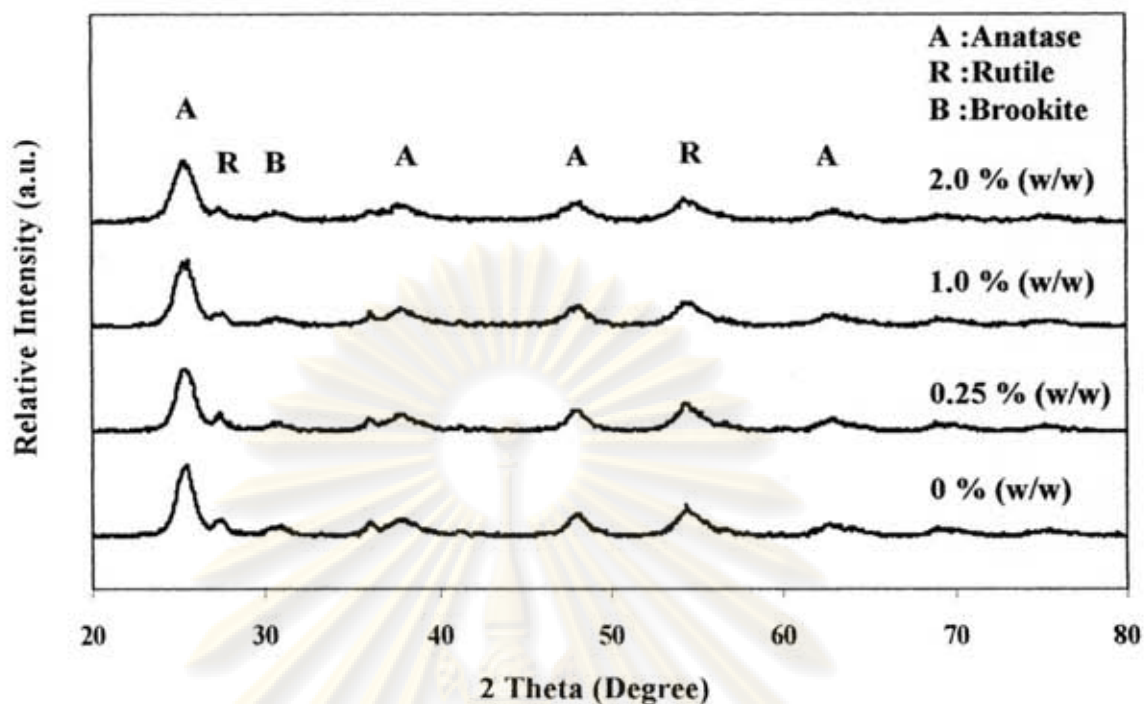


Figure 4.21 XRD patterns of CeO₂/TiO₂ powders at various percentage of Ce/Ti

Table 4.8 Crystal size, Surface area and weight fraction of anatase, rutile and brookite phase of CeO₂/TiO₂ powders sintered at 400°C for 2 h

Ce/Ti (wt%)	Crystal size (nm)	Surface area (m ² /g)	Amount of Ce from ICP (wt%)	W _A	W _R	W _B
0	7.3	88.1	-	0.58	0.16	0.26
0.25	6.4	106.5	0.24	0.60	0.16	0.24
1	6.1	114.5	0.91	0.60	0.16	0.24
2	5.6	127.5	1.82	0.57	0.12	0.31

W_A : weight fraction of anatase phase

W_R : weight fraction of rutile phase

W_B : weight fraction of brookite phase

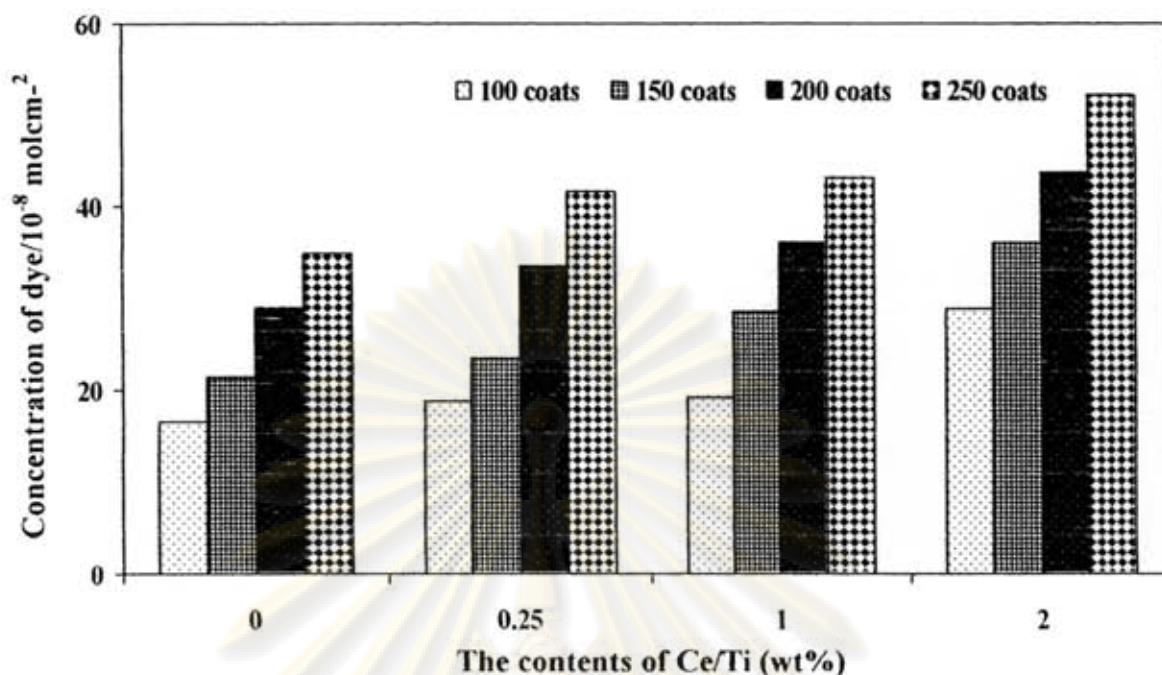


Figure 4.22 Relationship between concentrations of dye with various contents of Ce/Ti at different of number of coat of electrode

The result of PL intensity of 1.0 wt% Ce/Ti showed the highest intensity correlated with the lowest rate combination of electron and hole (were shown in Figure 4.22), it is the reason why optimum dosage of ceria was 1 wt%. The addition of ceria into titania plays an important role in the interfacial charge and elimination of electron-hole recombination (Li et al., 2005) and stable chemical state easily captures electrons to become another relatively stable chemical state with a half filled or full filled outer electronic structure (Liqiang et al., 2006).

The efficiencies of dye sensitized solar cells of CeO₂/TiO₂ electrode increase with increasing of film thickness were shown Figure 4.23 due to high surface area correlate with an amount of dye absorbed. At the same time the contents of ceria increase due to increasing of efficiency was found to be maximal up 1 wt% of ceria and it decrease cause the optimum of PL intensity occurred at 2 wt% of Ce/Ti.

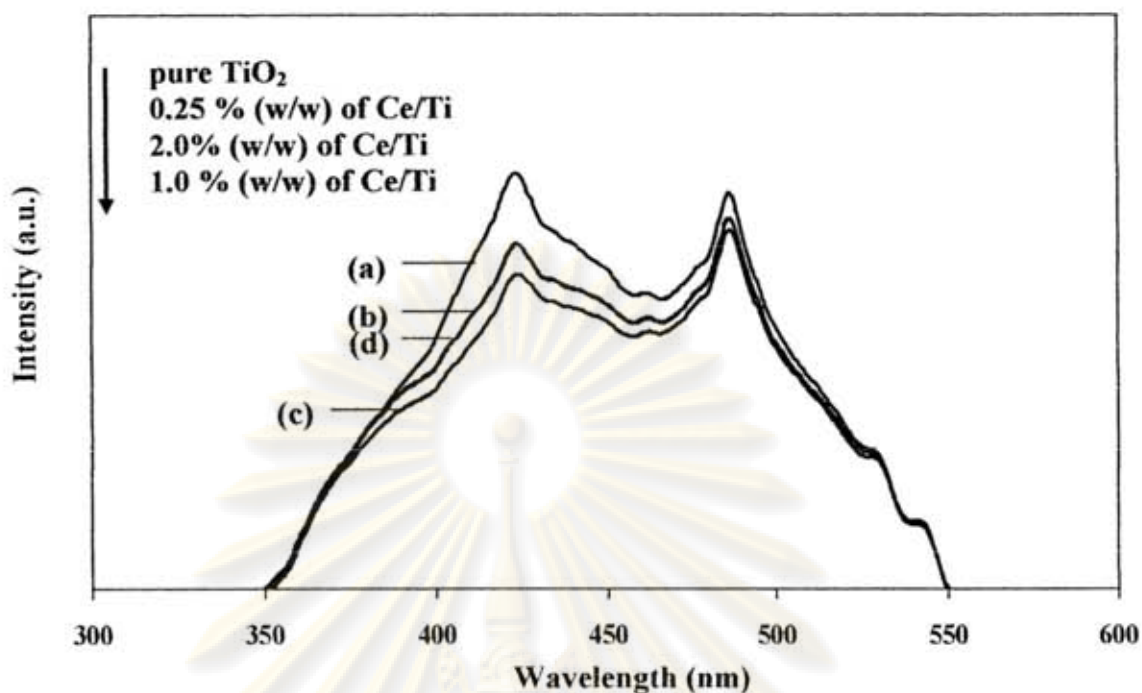


Figure 4.23 PL spectra of $\text{CeO}_2/\text{TiO}_2$ at various contents of (a) pure TiO_2 , (b) 0.25% (w/w) of Ce/Ti, (c) 1% (w/w) of Ce/Ti and (d) 2% (w/w) of Ce/Ti

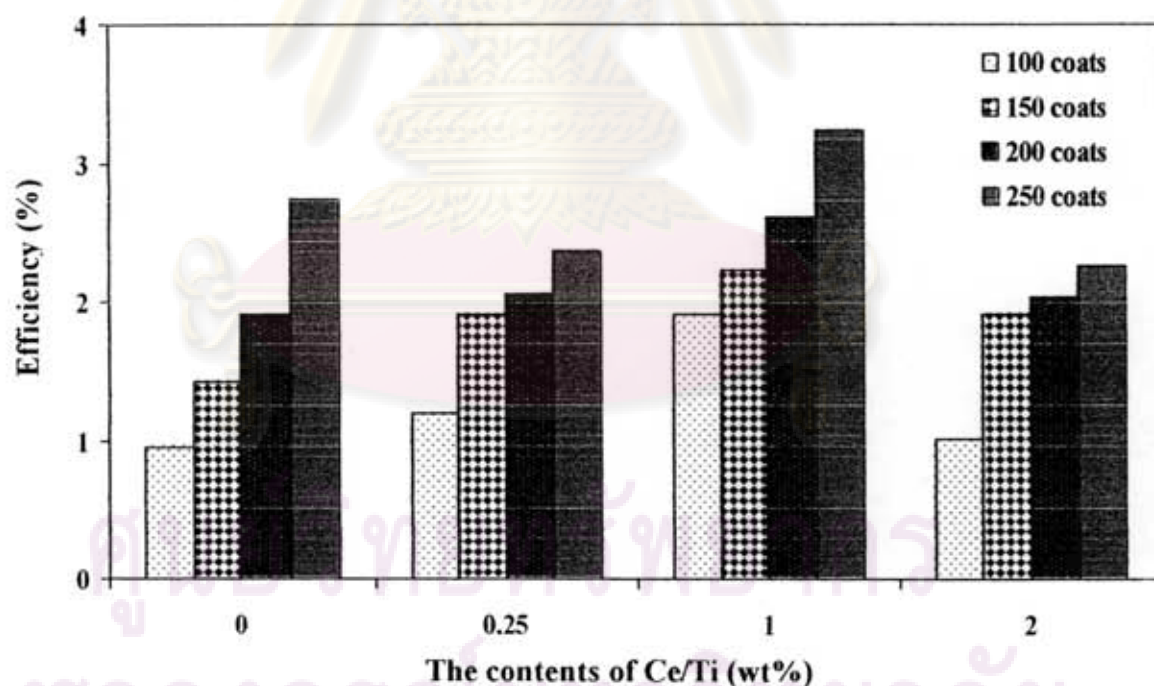


Figure 4.24 Efficiencies of dye sensitized solar cells of $\text{CeO}_2/\text{TiO}_2$ electrode calcined at 400°C at various number of coat and the contents of Ce/Ti

CHAPTER V

CONCLUSIONS AND RECOMMENDATIONS

In this chapter, section 5.1 provided the conclusions obtained from the experimental results of the effect of sintering temperature, thickness of film and the modified TiO₂ electrode by addition of Fe₂O₃, WO₃ and CeO₂. Additionally, recommendations for future study were given in section 5.2.

5.1 Conclusions

The sintering temperature affect on photocurrent-voltage characteristic which the increasing sintering temperature due to increase in the crystallinity which helps the electron transport and it improve of interconnection between particles. Beside, the increasing of film thickness related to high surface area due to increasing of the amount of dye absorbed to improve efficiency of cell. However, the increasing thickness of film correlated with the charge recombination, which limits the conversion efficiency.

The added of Fe₂O₃, WO₃ and CeO₂ into TiO₂ electrode role was based on the crystal growth inhibited leading to high surface area when compared with pure TiO₂ which resulted in the higher the amount of dye adsorbed. The addition of WO₃ and CeO₂ gave the I_{SC} higher pure TiO₂ which to improve efficiency of cell while the added of Fe₂O₃ due to the I_{SC} and the efficiency of cell decrease. The 1%wt of CeO₂TiO₂ electrode sintered at 400°C at number of coat was 250 gave the best efficiency of cell of 3.23 %.

ศูนย์วิทยทรัพยากร
จุฬาลงกรณ์มหาวิทยาลัย

5.2 Recommendations for future studies

From the previous conclusions, the following recommendations for future studies are proposed.

1. Improving efficiency of dye sensitized solar cell by optimizing fabrication procedure.
2. Modification of TiO_2 electrode layer by adding another metal oxide in TiO_2 layer.



ศูนย์วิจัยทรัพยากร
จุฬาลงกรณ์มหาวิทยาลัย

REFERENCES

- Baumann, A., Bhargava, Y., Liu, Z., Nemet, G., and Wilcox, J. Photovoltaic technology review [Online]. University of California at Berkeley: Available from: <http://www.socrates.berkeley.edu> [2008, February 11]
- Brammer, T. and Lu, M. Nanostructured titania dye sensitised solar cells: Study of the effects of variations in the TiO₂ film thickness and dyeing Times Nanomac University of Queensland (2004).
- Chiba, Y., Islam, A., Watanabe, Y., Komiya, R., Koide N., and Han, L. Dye-sensitized solar cells with conversion efficiency of 11.1%. Japanese Journal of Applied Physics 45 (2006): 638-640.
- Halme, J., Saarinen, J., and Lund, P. Spray deposition and compression of TiO₂ nanoparticle film for dye sensitized solar cells on plastic substrates. Solar Energy Materials & Solar Cells 90 (2006): 887–899.
- Higashimoto, S., Sakiyama, M., Azuma, M. Photoelectrochemical properties of hybrid WO₃/TiO₂ electrode. Effect of structures of WO₃ on charge separation behavior. Thin Solid Films 503 (2006): 201 – 206.
- Huang, C. Y., Hsua, Y. C., Chena, J. G., Suryanarayana, V., Leeb, K. M., and Ho, K.C. The effects of hydrothermal temperature and thickness of TiO₂ film on the performance of a dye-sensitized solar cell. Solar Energy Materials & Solar Cells 90 (2006): 2391–2397.
- Joshi, P., Xie, Y., Ropp, M., Galipeau, D., Bailey, S., and Qiao, Q. Dye-sensitized solar cells based on low cost nanoscale carbon/TiO₂ composite counter electrode. Energy & Environmental Science 2 (2008): 426-429.
- Kalyanasundaram, K. and Grätzel, M. Applications of functionalized transition metal complexes in photonic and optoelectronic devices. Chemical Reviews 177 (1998): 347-414.
- Kang, M.G., Ryu, K. S., Chang, S. H, Park, N. G., Hong, J. S., and Kim, K. J. Dependence of TiO₂ film thickness on photocurrent-voltage characteristics of dye-sensitized solar cells. Bull Korean Chemistry 25 (2004): 5.
- Kartini, I. Synthesis and characterisation of mesostructured titania for photoelectrochemical solar cells [Online]. University of Queensland: Available from: <http://www.cheque.uq.edu.au/ugrad/theses/> [2008, April 11]

- Karthikeyan, C. S., Thelakkat, M., and Willert-Porada, M. Different mesoporous titania film for solid-state dye sensitised solar cells. Thin Solid Film 511 – 512 (2006): 187–194.
- Kitiyanan, A. Kato, T., Suzuki, Y., and Yoshikawa, S. The use of binary $\text{TiO}_2\text{-GeO}_2$ oxide electrodes to enhanced efficiency of dye sensitized solar cells. Journal of Photochemistry and Photobiology A: Chemistry 179 (2005): 130–134.
- Kitiyanan, A. and Yoshikawa, S. The use of ZrO_2 mixed TiO_2 nanostructures as efficient dye sensitized solar cells' electrodes. Materials Letters 59 (2005): 4038-4040.
- Kitiyanan, A., Ngamsinlapasathian, S., Pavasupree, S., and Yoshikawa, S. The preparation and characterization of nanostructured $\text{TiO}_2\text{-ZrO}_2$ mixed oxide electrode for efficiency dye sensitized solar cells. Journal of Solid State Chemistry 178 (2005):1044–1048.
- Ko, K. H., Lee, Y. C., and Jung, Y. J. Enhanced efficiency of dye- sensitized TiO_2 solar cells (DSSC) by doping of metal ions. Journal of Colloid and Interface Science 283 (2005): 482–487.
- Lee, K., Suryanarayananb, V., and Hoa, K. A study on the electron transport properties of TiO_2 electrodes in dye sensitized solar cells. Solar Energy Materials & Solar Cells 91 (2007): 1416–1420.
- Lenzmann, F., and Kroon, J. Review: Recent Advances in Dye sensitized Solar Cells. Advances in OptoElectronics 10 (2007): 1755-1785.
- Li, Z., Yang, L., and Geb, K. Photocatalytic activity of $\text{WO}_x\text{-TiO}_2$ under visible light irradiation. Journal of Photochemistry and Photobiology A: Chemistry 141 (2001): 209–217.
- Li, F., Li, Z., Hou, F., Cheah, W., and Choy, H. Enhanced photocatalytic activity of $\text{Ce}^{3+}\text{-TiO}_2$ for 2-mercaptobenzothiazole degradation in aqueous suspension for odour control. Applied Catalysis A 285 (2005): 181–189.
- Liqianga, J., Yichuna, Q., Baiqia, W., Shudana, L., Baojianga, J., Libina, Y., Weia, F., Hongganga, F., and Jiamong, S. Review of photoluminescence performance of nano-sized semiconductor materials and its relationships with photocatalytic activity. Solar Energy Materials & Solar Cells 90 (2006):1773–1787.

- Ngamsinlapasathian, S., Sreethawong, T., Suzuki, Y., and Yoshikawa, S. Single- and double-layered mesoporous TiO₂/P25 TiO₂ electrode for dye sensitized solar cell. Solar Energy Materials & Solar Cells 86 (2005): 269–282.
- N-Park, G., Lagemaat, J., and Frank, A. Comparison of Dye sensitized Rutile- and Anatase-Based TiO₂ Solar Cells. The Journal of Physical chemistry B 104 (2000): 8989-8994.
- Thavasi, V., Renugopalakrishnan, V., Jose, R., and Ramakrishna, S. Controlled electron injection and transport at materials interfaces in dye sensitized solar cells. Materials Science and Engineering R 63 (2008): 81-89.
- Nelson, J. The Physics of Solar Cells Properties of Semiconductor Materials. 2nd ed. Singapore: Imperial College Press, 2004.
- O'Regan, B., and Grätzel, M. Low-cost high-efficiency solar cell based on dye sensitized colloidal TiO₂ films. Nature 353 (1991): 737-740.
- Phani, G., Tulloch, G., Vittorio, D., and Skryabin, I. Titania solar cells: new photovoltaic technology. Renewable Energy 22 (2001): 303-309.
- Porkodi, K., and Arokiamary, S. Synthesis and spectroscopic characterization of nanostructured anatase titania. Materials Characterization 58 (2007): 495–503.
- R-Jang, S., Vittal, R., Lee, J., Jeonga, N., and J-Kim, K. Linkage of N3 dye to N3 dye on nanocrystalline TiO₂ through trans-1,2-bis(4-pyridyl)ethylene for enhancement of photocurrent of dye sensitized solar cells. Chemical Communications (2005): 103-105.
- Su, C., Hong, B., and Tseng, C. Sol-gel preparation and photocatalysis of titanium dioxide. Catalysis Today 96 (2004): 119-126.
- Wu, Y., Zhang, J., Xiao, L., and Chen, F. Preparation and characterization of TiO₂ photocatalysts by Fe³⁺ doping together with Au deposition for the degradation of organic pollutants. Applied Catalysis B: Environmental 88 (2008): 525-532.
- Yoshikawa, S., Kitiyanan, A., Ngamsinlapasathian, S., Yoshikawa, O., and Suzuki, Y. The enhancement of dye sensitized solar cell performance by TiO₂-based mixed metal oxide nanostructured electrodes. Photovoltaic Energy Conversion, Conference Record of the 2006 IEEE 4th World Conference 1 (2006): 279-282.
- Zhang, H., and Banfield, F. Understanding polymorphic phase transformation behavior during growth of nanocrystalline aggregates: insights from TiO₂. The Journal of Physical chemistry B 104 (2000): 8486-8494.

Zhang, J., Boyd, Ian W., O' Sullivan, B.J., Hurley, P.K., Kelly, P.V., and Sénateur, J.P. Nanocrystalline TiO₂ films studied by optical, XRD and FTIR spectroscopy. The Journal of crystalline solids 303 (2002): 134-138.

Zhao, D., Peng, T., Lu, L., Cai, P., Jiang, P., and Bian, Z. Effect of annealing temperature on the photoelectrochemical properties of dye sensitized solar cells made with mesoporous TiO₂ nanoparticles. The Journal of Physical chemistry C 112 (2008): 8486-8494.



ศูนย์วิทยทรัพยากร
จุฬาลงกรณ์มหาวิทยาลัย



APPENDICES

ศูนย์วิทยทรัพยากร
จุฬาลงกรณ์มหาวิทยาลัย

APPENDIX A

CALCULATION OF THE CRYSTALLITE SIZE

Calculation of the crystallite size by Debye-Scherrer equation

The crystallite size can be calculated from the width at half-height of the diffraction peak of XRD pattern using the Debye-Scherrer equation.

From Scherrer equation:

$$D = \frac{\kappa \lambda}{\beta \cos \theta} \quad (\text{A.1})$$

- where
- D = Crystallite size, Å
 - K = Crystallite-shape factor = 0.9
 - λ = X-ray wavelength, 1.5418 Å for CuK α
 - θ = Observed peak angle, degree
 - β = X-ray diffraction broadening, radian

The X-ray diffraction broadening (β) is the pure width of a powder diffraction, free of all broadening due to the experimental equipment. Standard α -alumina is used to observe the instrumental broadening since its crystallite size is larger than 2000 Å. The X-ray diffraction broadening (β) can be obtained by using Warren's formula.

From Warren's formula:

$$\beta^2 = B_M^2 - B_S^2 \quad (\text{A.2})$$

$$\beta = \sqrt{B_M^2 - B_S^2}$$

- Where
- B_M = Measured peak width in radians at half peak height.
 - B_S = Corresponding width of a standard material.

Example: calculation of the crystallite size of titania

$$\text{The half-height width of (101) diffraction peak} = 1.31583^\circ$$

$$= 0.02297 \text{ radian}$$

$$\text{The corresponding half-height width of peak of titania} = 0.003831 \text{ radian}$$

$$\text{The pure width} = \sqrt{B_w^2 - B_s^2}$$

$$= \sqrt{0.02297^2 - 0.003831^2}$$

$$= 0.02264 \text{ radian}$$

$$\beta = 0.02264 \text{ radian}$$

$$2\theta = 25.32^\circ$$

$$\theta = 12.66^\circ$$

$$\lambda = 1.5418 \text{ \AA}$$

$$\text{The crystallite size} = \frac{0.9 \times 1.5418}{0.02264 \cos 12.66} = 62.25 \text{ \AA}$$

$$= 6.3 \text{ nm}$$

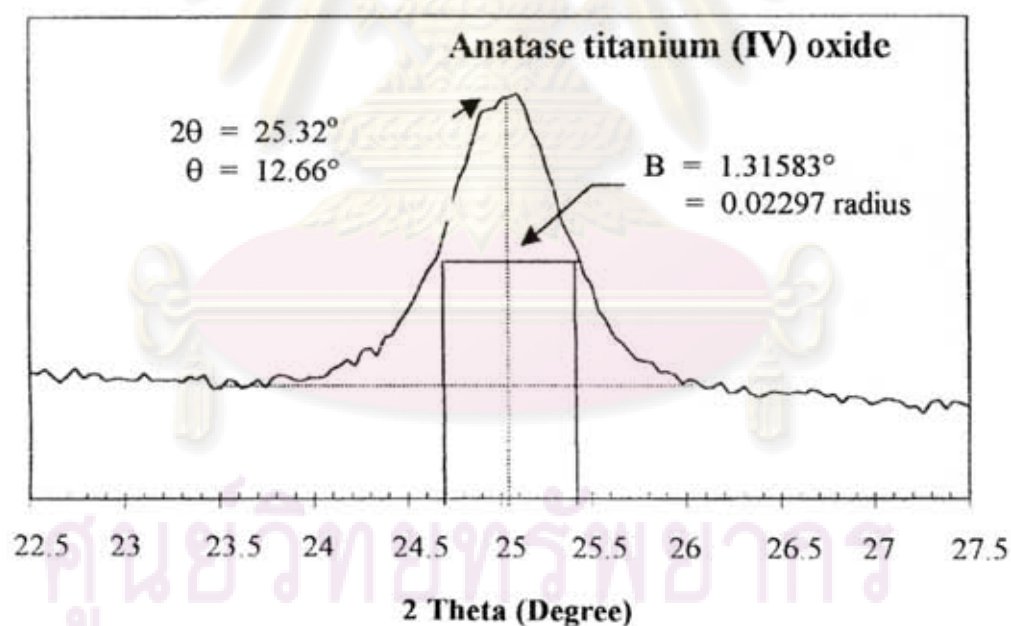


Figure A.1 The (101) diffraction peak of titania for calculation of the crystallite size

APPENDIX B

CALCULATION OF WEIGHT FRACTION OF ANATASE, RUTILE AND BROOKITE PHASE

The phase content of a sample were determined by XRD which can be calculated from the integrated intensities at 2θ values of 25.32° , 27.44° and 30.88° corresponded to the anatase, rutile and brookite phase, respectively.

The weight fraction of the phase content can be calculated by (Zhang and Banfield, 2000) as follows:

$$W_A = \frac{k_A A_A}{k_A A_A + A_R + k_B A_B}$$

$$W_R = \frac{A_R}{k_A A_A + A_R + k_B A_B}$$

$$W_B = \frac{k_B A_B}{k_A A_A + A_R + k_B A_B}$$

Where

W_A = weight fraction of anatase

W_R = weight fraction of rutile

W_B = weight fraction of brookite

A_A = the intensity of the anatase peak

A_R = the intensity of rutile peak

A_B = the intensity of the brookite peak

k_A = the coefficients factor of anatase was 0.886

k_B = the coefficients factor of rutile was 2.721

Example: calculation of the phase contents of TiO_2 sintered 300°C

Where

The integrated intensities of anatase (A_A) = 789

The integrated intensities of rutile (A_R) = 158

The integrated intensities of brookite (A_B) = 111

The weight fraction of the phase content can be calculated by (Zhang and Banfield, 2000) as follows:

$$W_A = \frac{0.886(789)}{0.886(789) + (158) + 2.721(111)} = 0.60$$

$$W_R = \frac{158}{0.886(789) + (158) + 2.721(111)} = 0.14$$

$$W_B = \frac{2.721(111)}{0.886(789) + (158) + 2.721(111)} = 0.26$$

ศูนย์วิทยทรัพยากร
จุฬาลงกรณ์มหาวิทยาลัย

APPENDIX C

**DETERMINATION OF THE AMOUNT OF DYE ADSORBED ON
TITANIA SURFACE**

The amount of dye adsorbed was determined by UV-Visible Absorption Spectroscopy (UV-Vis) where measuring the concentration of dye desorbed on the titania film into a mixed solution of 0.1M NaOH and ethanol (1:1 in volume fraction).

The calibration curve of the concentration of dye with absorbance was illustrated in the following figure.

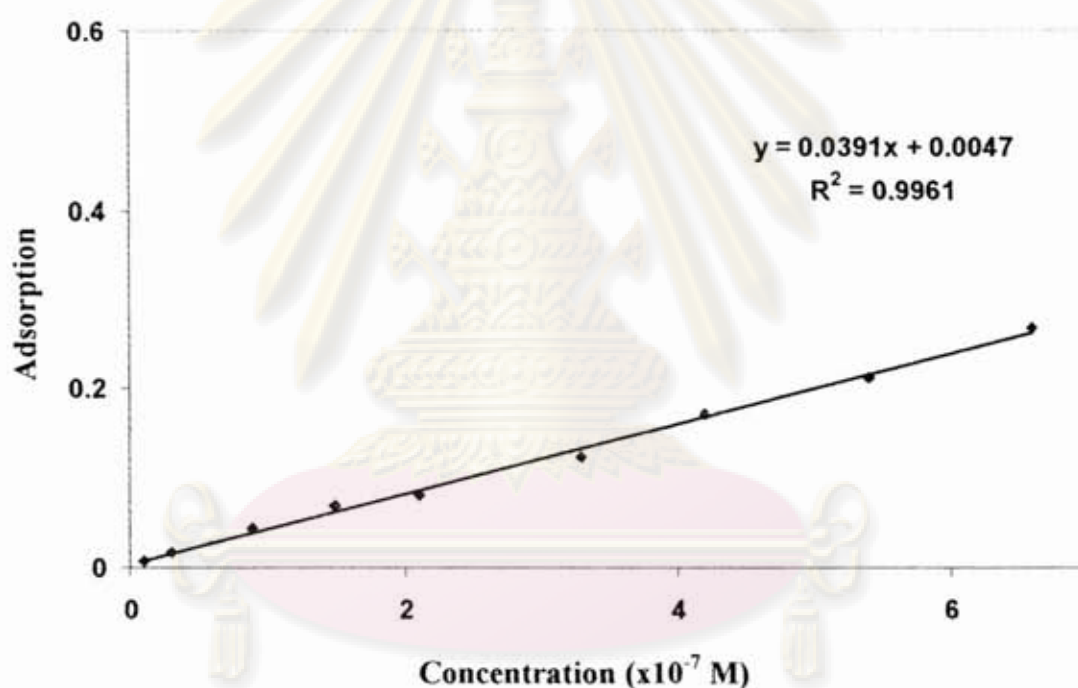


Figure C.1 The calibration curve of the concentration of dye adsorbed on titania

ศูนย์วิจัยทันตวิทยา
จุฬาลงกรณ์มหาวิทยาลัย

APPENDIX D

CALCULATION OF RESULT OF ICP-OES

Calculation of ICP-OES results

The results from ICP-OES characterization were calculated the contents of metal in catalysts. The example of calculation is as following:

Example: calculation of the contents of 0.25 wt% of Ce/Ti in CeO₂/TiO₂ powder.

For 0.25 wt% of Ce/Ti powder, the initial weight of powder was 0.0173 g. Hence, the calculation of the ceria contents the catalysts as follows:

The amounts of ceria in the catalyst were;

$$\begin{aligned} \text{In 100 g of the Ce/TiO}_2, \text{ had a ceria content was } & 0.25 \text{ g} \\ \text{In 0.0173 g of the Ce/TiO}_2, \text{ had a ceria content was } & \frac{0.0173 \times 0.25}{100} \\ & = 0.00004325 \text{ g} \\ & = 0.04325 \text{ mg} \end{aligned}$$

For digest a samples were diluted to 100 cm³ of volume

Therefore;

$$\text{The sample had a concentration were } = \frac{0.04325 \times 1000}{100} = 0.4325 \text{ ppm}$$

From the results of ICP-OES, shown the contents of ceria was 0.4233 ppm

Therefore;

The ceria contents in the catalysts were calculated by

The ceria concentrations were 0.4233 ppm refer 0.25 %wt of ceria in catalyst.

$$\begin{aligned} \text{The ceria concentrations were 0.4233 ppm refer } & \frac{0.4233 \times 0.25}{0.4325} \\ & = 0.24 \text{ wt\% of ceria in the catalyst.} \end{aligned}$$

APPENDIX E

**THE ELECTROCHEMICAL PROPERTIES OF
DYE SENSITIZED SOLAR CELL**

The electrochemical properties of dye sensitized solar cells as a film thickness and sintering temperature of TiO₂ electrode by I-V tester. In this study three samples were used, and the efficiency of cell given is the average value follow by the standard derivation.

Table E.1 The electrochemical properties of TiO₂ electrode calcined at 300°C with various numbers of coats

Numbers of coats	V _{OC} (Volt)	I _{SC} (mA/cm ²)	Fill Factor	Efficiency (%)
100	0.69	1.79	0.60	0.73±0.04
150	0.70	2.28	0.67	1.07±0.12
200	0.69	2.72	0.66	1.23±0.12
250	0.68	2.76	0.69	1.31±0.04

Table E.2 The electrochemical properties of TiO₂ electrode calcined at 400°C with various numbers of coats

Numbers of coats	V _{OC} (Volt)	I _{SC} (mA/cm ²)	Fill Factor	Efficiency (%)
100	0.75	1.93	0.65	0.95±0.11
150	0.76	2.67	0.70	1.42±0.02
200	0.74	3.53	0.73	1.91±0.08
250	0.73	4.62	0.81	2.74±0.21

จุฬาลงกรณ์มหาวิทยาลัย

Table E.3 The electrochemical properties of TiO₂ electrode calcined at 500°C with various numbers of coats

Numbers of coats	V _{oc} (Volt)	I _{sc} (mA/cm ²)	Fill Factor	Efficiency (%)
100	0.72	1.67	0.63	0.85±0.15
150	0.68	2.21	0.69	1.02±0.07
200	0.71	2.72	0.72	1.41±0.05
250	0.70	4.28	0.78	2.36±0.03

Table E.4 The electrochemical properties of TiO₂ electrode calcined at 600°C with various numbers of coats

Numbers of coats	V _{oc} (Volt)	I _{sc} (mA/cm ²)	Fill Factor	Efficiency (%)
100	0.78	1.21	0.60	0.62±0.10
150	0.76	1.92	0.68	0.99±0.04
200	0.72	1.92	0.71	1.40±0.05
250	0.72	2.82	0.70	1.42±0.06

Table E.5 The electrochemical properties of 0.25 wt% Fe₂O₃/TiO₂ electrode calcined at 400°C at various numbers of coats

Number of coats	V _{oc} (Volt)	I _{sc} (mA/cm ²)	Fill Factor	Efficiency (%)
100	0.49	0.49	0.60	0.14±0.04
150	0.50	0.51	0.54	0.18±0.03
200	0.48	0.64	0.64	0.20±0.09
250	0.49	0.86	0.61	0.26±0.03

จุฬาลงกรณ์มหาวิทยาลัย

Table E.6 The electrochemical properties of 1.0 wt% Fe₂O₃/TiO₂ electrode calcined at 400°C at various numbers of coats

Number of coats	V _{oc} (Volt)	I _{sc} (mA/cm ²)	Fill Factor	Efficiency (%)
100	0.45	0.15	0.73	0.05±0.01
150	0.62	0.15	0.71	0.08±0.05
200	0.62	0.17	0.72	0.09±0.07
250	0.58	0.40	0.54	0.15±0.03

Table E.7 The electrochemical properties of 2.0 wt% Fe₂O₃/TiO₂ electrode calcined at 400°C at various numbers of coats

Number of coats	V _{oc} (Volt)	I _{sc} (mA/cm ²)	Fill Factor	Efficiency (%)
100	0.43	0.10	0.54	0.02±0.01
150	0.42	0.11	0.59	0.04±0.02
200	0.62	0.13	0.71	0.06±0.02
250	0.45	0.10	1.04	0.05±0.01

Table E.8 The electrochemical properties of 0.25 wt% WO₃/TiO₂ electrode calcined at 400°C at various numbers of coats

Number of coats	V _{oc} (Volt)	I _{sc} (mA/cm ²)	Fill Factor	Efficiency (%)
100	0.70	3.27	0.68	1.54±0.04
150	0.70	3.47	0.71	1.73±0.13
200	0.70	3.62	0.68	1.72±0.08
250	0.69	2.72	0.66	1.23±0.12

จุฬาลงกรณ์มหาวิทยาลัย

Table E.9 The electrochemical properties of 1.0 wt% WO₃/TiO₂ electrode calcined at 400°C at various numbers of coats

Number of coats	V _{oc} (Volt)	I _{sc} (mA/cm ²)	Fill Factor	Efficiency (%)
100	0.73	3.31	0.75	1.82±0.12
150	0.75	3.81	0.78	2.03±0.10
200	0.67	4.46	0.60	1.79±0.08
250	0.67	3.00	0.56	1.13±0.07

Table E.10 The electrochemical properties of 2.0 wt% WO₃/TiO₂ electrode calcined at 400°C at various numbers of coats

Number of coats	V _{oc} (Volt)	I _{sc} (mA/cm ²)	Fill Factor	Efficiency (%)
100	0.68	2.76	0.69	1.31±0.03
150	0.68	2.97	0.77	1.57±0.05
200	0.68	2.09	0.72	1.02±0.02
250	0.67	2.16	0.71	1.03±0.11

Table E.11 The electrochemical properties of 0.25 wt% CeO₂/TiO₂ electrode calcined at 400°C at various numbers of coats

Number of coats	V _{oc} (Volt)	I _{sc} (mA/cm ²)	Fill Factor	Efficiency (%)
100	0.72	2.48	0.66	1.19±0.10
150	0.69	3.21	0.87	1.91±0.12
200	0.71	3.87	0.74	2.05±0.11
250	0.70	4.28	0.78	2.36±0.02

จุฬาลงกรณ์มหาวิทยาลัย

Table E.12 The electrochemical properties of 1.0 wt% CeO₂/TiO₂ electrode calcined at 400°C at various numbers of coats

Number of coats	V _{oc} (Volt)	I _{sc} (mA/cm ²)	Fill Factor	Efficiency (%)
100	0.74	3.53	0.73	1.91±0.10
150	0.73	4.21	0.72	2.23±0.10
200	0.70	4.51	0.84	2.60±0.08
250	0.63	5.63	0.82	3.23±0.06

Table E.13 The electrochemical properties of 2.0 wt% CeO₂/TiO₂ electrode calcined at 400°C at various numbers of coats

Number of coats	V _{oc} (Volt)	I _{sc} (mA/cm ²)	Fill Factor	Efficiency (%)
100	0.70	2.07	0.69	1.01±0.04
150	0.68	3.31	0.75	1.90±0.05
200	0.68	3.81	0.74	2.03±0.09
250	0.69	4.23	0.75	2.25±0.10

ศูนย์วิจัยทรัพยากร
จุฬาลงกรณ์มหาวิทยาลัย

APPENDIX F

LIST OF PUBLICATIONS

Yasunun Wattanasurawit and Akawat Sirisuk. "Dye sensitized solar cell with WO_3/TiO_2 electrode layer", 2nd SUT Graduate Conference, Suranaree University of Technology, Nakhon Ratchasima, Thailand, January 21-22, 2009.



ศูนย์วิทยทรัพยากร
จุฬาลงกรณ์มหาวิทยาลัย

VITA

Miss Yasunun Wattanasurawit was born on March 11th, 1983 in Nakornsithumarat province, Thailand. She received the Bachelor Degree of Chemistry from Faculty of Science, King Mongkut's University of Technology North Bangkok, in 2004. She pursued her Master's study at Chulalongkorn University, Bangkok in June 2006.



ศูนย์วิทยทรัพยากร
จุฬาลงกรณ์มหาวิทยาลัย